PKA and PDE4D3 anchoring to AKAP9 provides distinct regulation of cAMP signals at the centrosome

Anna Terrin[1], Stefania Monterisi[2], Alessandra Stangherlin[1], Anna Zoccarato[1], Andreas Koschinski[2], Nicoletta C. Surdo[2], Marco Mongillo[3], Akira Sawa[4], Niove E Jordanides[5], Joanne C. Mountford[5] and Manuela Zaccolo[1,2*]

[1]Institute of Neuroscience and Psychology and [5]Institute of Cardiovascular and Medical Sciences, College of Medical, Veterinary and Life Sciences, University of Glasgow, UK; [2]Department of Physiology, Anatomy and Genetics, Oxford University, UK; [3]Venetian Institute of Molecular Medicine (VIMM), Padova, Italy; [4]Department of Psychiatry, Johns Hopkins University School of Medicine, MD 21287, USA

*Corresponding author:

Manuela Zaccolo, MD

Department of Physiology, Anatomy & Genetics

Sherrington Building, Parks Road

Oxford OX1 3PT, UK.

Email:- manuela.zaccolo@dpag.ox.ac.uk

Phone:- +44-(0)141-330-272530

Fax:- +44-(0)141-330-5481

Running title: Unique PKA signaling at the centrosome

eTOC Summary Statement: Control of cell cycle progression relies on unique regulation of centrosomal cAMP/PKA signals through PKA and PDE4D3 interaction with the A-kinase anchoring protein AKAP9.

Number of characters: 39249

Abstract

Previous work has shown that the PKA-regulated phosphodiesterase PDE4D3 binds to A-kinase anchoring proteins. One such protein, AKAP9, localizes to the centrosome. Here, we investigate whether a PKA-PDE4D3-AKAP9 complex can generate spatial compartmentalization of cAMP signaling at the centrosome. Real-time imaging of FRET reporters shows that centrosomal PDE4D3 modulated a dynamic microdomain within which cAMP concentration selectively changed over the cell cycle. AKAP9-anchored, centrosomal PKA showed a reduced activation threshold as a consequence of increased auto-phosphorylation of its regulatory subunit at S114. Finally, disruption of the centrosomal cAMP microdomain by local displacement of PDE4D3 impaired cell cycle progression due to accumulation of cells in prophase. Our findings describe a novel mechanism of PKA activity regulation that relies on binding to AKAPs and consequent modulation of the enzyme activation threshold rather than on overall changes in cAMP levels. Further, we provide for the first time direct evidence that control of cell cycle progression relies on unique regulation of centrosomal cAMP/PKA signals.

Introduction

The second messenger cAMP mediates the intracellular response to multiple hormones and neurotransmitters and regulates a wide variety of cellular processes including gene expression, metabolism and cell growth and division (Stork and Schmitt, 2002). cAMP is generated from ATP by adenylyl cyclases (ACs) and phosphodiesterases (PDEs) provide the only means to degrade cAMP (Conti and Beavo, 2007). PDEs therefore play a key role in the control of cAMP resting levels as well as in determining the amplitude and duration of cAMP signals in response to extracellular stimuli (Houslay, 2010). The main effector of cAMP is protein kinase A (PKA), a tetrameric enzyme that in its inactive form consists of two catalytic subunits (C) and one regulatory subunit (R) dimer. Upon binding of cAMP to the R subunits the C subunits are released and phosphorylate downstream targets.

A multitude of different stimuli can generate an increase in intracellular cAMP and active PKA C subunits can potentially phosphorylate a large variety of protein targets within the same cell. However, in order for the cell to execute the appropriate task in response to a specific stimulus, the correct subset of downstream targets must be phosphorylated. To achieve this, spatial confinement (compartmentalization) of the molecular components of the cAMP signaling pathway is critical (Zaccolo, 2009). PKA is tethered to subcellular loci via binding to A-kinase anchoring proteins (AKAPs). AKAPs anchor PKA in proximity to its targets via binding to the amino-terminal dimerization/docking (D/D) domains of PKA R subunits of an amphipatic helix within the AKAP sequence (Wong and Scott, 2004). The cAMP signal is also compartmentalized,

with different intracellular sub-compartments showing different concentrations of the second messenger (Zaccolo and Pozzan, 2002). Different subsets of anchored PKA are thus exposed to different levels of cAMP, resulting in selective activation and phosphorylation of the appropriate subset of targets (Di Benedetto et al., 2008). PDEs, a large super-family of enzymes comprised of 11 families (PDE1-11) and more than 30 isozymes, can also be localized to specific subcellular compartments and, by locally degrading cAMP, play a key role in the spatial control of cAMP signals propagation (Mongillo et al., 2004). Long isoforms of the PDE4 family, including PDE4D3, can be phosphorylated and activated by PKA (Sette and Conti, 1996; MacKenzie et al., 2002) and members of the PDE4D subfamily have been shown to interact with a number of AKAPs, including AKAP6 (Dodge et al., 2001), AKAP7 (Stefan et al., 2007) and AKAP9 (Tasken et al., 2001). The presence of PKA and PDE4D3 within the same macromolecular complex may thus provide a negative feedback system where elevated cAMP concentrations trigger PKA to phosphorylate and activate PDE4, reducing local cAMP levels and resetting PKA activity selectively at that site (Dodge et al., 2001).

AKAP9/450/350/CG-NAP (hereafter referred to as AKAP450) localizes at the centrosome (Schmidt et al., 1999; Takahashi et al., 1999; Witczak et al., 1999) through a conserved protein interaction module known as the pericentrin-AKAP350 centrosomal targeting (PACT) domain (Gillingham and Munro, 2000). Localization of AKAP450 at the centrosome has been shown to be required for centrosome integrity and centriole duplication (Keryer et al., 2003).

The centrosome plays a key role in cell cycle progression and acts as a scaffold for the accumulation and interaction of different cell cycle regulators (Cuschieri et al., 2007). PKA has been shown to be involved in many aspects of cell cycle regulation including centrosome duplication, S-phase, G_2 arrest, mitotic spindle formation, exit from M-phase and cytokinesis (Matyakhina et al., 2002), however which, if any, of these functions is regulated by a PKA subset targeted at the centrosome remains to be established. In addition, it is not clear how cells achieve appropriate control of cell proliferation while continuously being exposed to hormonal fluctuations and, consequently, to changes in intracellular cAMP levels.

In this study we use real time imaging and a combination of FRET-based reporters to explore the hypothesis that anchoring of PKA and PDE4D3 to AKAP450 provides a structural basis for selective regulation of cAMP signals at the centrosome. Our results show, for the first time, that the centrosome is a subcellular compartment undergoing a sophisticated and dynamic control of cAMP signals and PKA activation that relies on PKA anchoring to AKAP450 and on the presence of PDE4D3 and can be independent of overall changes of cAMP levels in the cytosol. In addition, we show that selective disruption of cAMP/PKA signaling at the centrosome has unique effects on cell cycle progression.

Results

To study cAMP signals at the centrosome we generated a Chinese Hamster Ovary (CHO) cell clone that stably expresses a PKA-based FRET sensor, PKA-GFP (Vaasa et al., 2010). The sensor includes the regulatory type II (RII-CFP) and the catalytic (C-YFP) subunits of PKA tagged, at their carboxyl-termini, with the cyan and the yellow variants of the green fluorescent protein, respectively (**Fig. 1A**) (Zaccolo et al., 2000). In the absence of cAMP the sensor subunits RII-CFP and C-YFP interact, allowing energy transfer (FRET) from the donor CFP to the acceptor YFP. In the presence of cAMP, the RII-CFP and C-YFP subunits dissociate and FRET is abolished (**Fig. 1A**). We have previously reported that PKA-GFP shows the same cAMP-dependence and the same sensitivity to cAMP and ability to phosphorylate substrate as wild-type PKA (Mongillo et al., 2004) and interacts with endogenous AKAPs via the D/D domain of its RII-CFP subunits (Zaccolo and Pozzan, 2002). Expression of PKA-GFP in CHO cells shows a clear localization of the sensor at the centrosome both in interphase cells and in mitotic cells (**Fig. 1B**) without affecting centrosome morphology (**Suppl. Fig 1**). Centrosomal localization of the sensor is confirmed by co-localization of RII-CFP with the centrosomal marker γ-tubulin (**Fig, 1C,** and **Suppl. Fig 1**). Immuno-staining with CTR453, a monoclonal antibody specific for AKAP450 (Keryer et al., 2003; Bailly et al., 1989) shows co-localization of PKA-GFP and AKAP450 at the centrosome (**Fig. 1C**). To assess whether the centrosomal localization of the sensor is mediated by interaction with centrosomal AKAPs, a red fluorescent protein (RFP)-tagged RII subunit was co-expressed with either GFP-tagged SuperAKAP-IS or GFP-tagged RIAD. The peptides RIAD (Carlson et al., 2006) and SuperAKAP-IS (Gold et al., 2006) compete selectively

with the binding of RI and RII to AKAPs, respectively. As shown in **Fig. 1D**, co-expression of SuperAKAP-IS GFP, but not RIAD GFP, completely abolishes the centrosomal localization of RII-RFP.

Basal cAMP levels are lower at the centrosome than in the bulk cytosol in interphase cells. CHO cells expressing the PKA-GFP sensor show a small but highly significant difference in the basal CFP/YFP emission intensity ratio (R) at the centrosome as compared to the bulk cytosol (**Fig. 2A**), indicating that in resting, non-stimulated interphase cells the level of cAMP at the centrosome is lower than the average cAMP level in the cytosol.

A similar difference between bulk cytosol and centrosome was detected by RII_epac (**Suppl. Fig. 2A**), a unimolecular FRET reporter for cAMP carrying at its amino-terminus the D/D domain from the RII subunit of PKA (Di Benedetto et al., 2008) and therefore, similarly to PKA-GFP, able to interact with endogenous centrosomal AKAPs **(Fig. 2B**). The RII_epac reporter detects a significant difference between cytosolic and centrosomal basal cAMP levels in a number of other cell types analyzed, including the macrophage cell line RAW264.7, the human neuroblastoma cell line SH-SY5Y(Biedler et al., 1978), primary human olfactory neurons (HON), primary rat cardiac fibroblasts (RCF) (**Fig. 2C**) and the non-transformed cell line RPE1 (**Suppl. Fig 3A**).

PDE4D3 is responsible for the low basal cAMP level at the centrosome. In a variety of cell types, including CHO cells (**Suppl. Fig. 4A**) and RPE1 (**Suppl. Fig. 3B**) PDE4D3 localizes to the centrosome and has been shown to bind to AKAP450 (McCahill et al., 2005; Tasken et al., 2001). Anchoring of PDE4D3 at the centrosome may therefore

explain the observed low cAMP level at this site. In support of this hypothesis, selective inhibition of PDE4 enzymes with 10 μM rolipram completely abolished the difference in cAMP between the centrosome and the bulk cytosol as detected by both PKA-GFP and RII_epac (**Fig. 3A-C**). In contrast, selective inhibition of PDE2 with 10 μM EHNA (**Fig. 3D, E**) or selective inhibition of PDE3 with 10 μM cilostamide (**Fig. 3F**) did not affect the gradient between centrosome and cytosol. In further support of a role of PDE4D3 in maintaining a low basal cAMP level at the centrosome, genetic knock down of PDE4D using a small RNA interference approach and resulting in an almost complete ablation of all PDE4D isozymes (**Suppl. Fig. 4B**) completely abolished the differences in cAMP levels between cytosol and centrosome (**Fig. 3G-H**) whereas the control oligonucleotide siGLO did not show any effect (**Fig. 3I**). Anchoring of active PDE4D3 at the centrosome appears to be necessary to maintain low the local cAMP concentration as shown by experiments where we used a catalytically-inactive mutant of PDE4D3 (dnPDE4D3) (McCahill et al., 2005). When over-expressed, dnPDE4D3 localizes at the centrosome (**Suppl. Fig. 4C**) and is expected to displace endogenous active PDE4D3 from its centrosomal anchor sites. Over-expression of dnPDE4D3 in CHO cells completely abolished the difference in cAMP concentration between the centrosome and the cytosol, as detected by the co-expressed PKA-GFP (**Fig. 3J-K**). In contrast, over-expression of a catalytically-inactive mutant of a different PDE4 isozyme, (dnPDE4A4, **Suppl. Fig. 4C**) (McCahill et al., 2005) did not affect the cAMP gradient between cytosol and centrosome (**Fig. 3L**). Taken together the above data strongly indicate that PDE4D3 is responsible for maintaining a microdomain with low cAMP concentration at the centrosome.

PKA anchored to AKAP450 shows increased sensitivity to cAMP. We next assessed the cAMP response generated in the bulk cytosol and at the centrosome upon activation of ACs with forskolin, using either the RII_epac or the PKA-GFP reporter. Upon application of 25 μM forskolin we found that the RII_epac sensor reported an equal FRET change in the cytosol and at the centrosome (**Fig. 4A**) whereas, unexpectedly, the PKA-GFP reporter recorded a significantly higher signal at the centrosome than in the bulk cytosol (**Fig. 4B**). To explain this discrepancy, we hypothesized that the higher FRET change recorded at the centrosome by PKA-GFP may be the consequence of an increased sensitivity to cAMP of the centrosomal targeted PKA-based biosensor. To verify this hypothesis we expressed the PKA-GFP sensor in CHO cells in combination with a fragment of the centrosomal AKAP450 encompassing amino acids 933-1804 (AKAP450-2) (Witczak et al., 1999) and including the amphipatic helix responsible for binding the RII subunits of PKA. AKAP450-2 lacks the PACT domain responsible for anchoring of AKAP450 to the centrosome (Gillingham and Munro, 2000) (**Suppl. Fig. 2B**). Thus, when expressed in cells, AKAP450-2 is a cytosolic polypeptide (**Fig. 4C**) that retains its ability to bind to PKA RII subunits (**Fig. 4D**). The rationale for this experiment is that if anchoring of PKA to endogenous AKAP450 at the centrosome affects the kinase sensitivity to cAMP, the same effect should result from PKA binding to AKAP450-2 in the cytosol. **Fig 4E** shows that this is the case and, as reported in **Fig. 4F**, the dose-response curve where FRET change is plotted against increasing concentrations of forskolin shows a shift to the left for cells co-expressing the FRET sensor and AKAP450-2, confirming that a lower concentration of cAMP is sufficient to dissociate PKA-GFP when it is bound to AKAP450. The effect of

AKAP450-2 on the sensitivity of PKA-GFP to cAMP is completely abolished in the presence of SuperAKAP-IS (**Fig. 4G**), confirming that this effect depends on the interaction of PKA-GFP with AKAP450-2. AKAP450-2 has no effect on the FRET change detected by a variant of the PKA-GFP sensor (ΔPKA-GFP) in which the D/D domain of the RII subunit has been deleted (Zaccolo and Pozzan, 2002), thereby resulting in a sensor that cannot bind to AKAPs (**Fig. 4H**) or when a serine to proline substitution (S1451P) is introduced in AKAP450-2 (*mut*AKAP450-2) that disrupts the amphipatic helix and abolishes the ability of PKA-GFP to bind (Feliciello et al., 2001); (Alto et al., 2003) (**Fig. 4I**). As an additional control, we measured the FRET change reported by the sensor RII_epac when co-expressed with the AKAP450-2 fragment and we found no difference compared to the FRET change recorded in the presence of the sensor alone (**Fig. 4J**). The increased sensitivity to cAMP appears to be specific for PKA enzymes anchored to AKAP450 as co-expression of PKA-GFP with fragments from Rt31 (Klussmann et al., 2001), AKAP79 (Herberg et al., 2000) or AKAP149 (Carlson et al., 2003), all including the RII-binding amphipatic helix, did not result in a significant difference in the FRET response compared to control cells expressing the sensor alone (**Fig.4K-M).** Overall, the above data show that anchoring of PKA to AKAP450 results in an increased sensitivity of the FRET signal to cAMP, which is indicative of a reduced activation threshold of PKA.

Binding of PKA to AKAP450 results in increased phosphorylation activity. To establish whether anchoring of PKA to AKAP450 affects PKA-mediated phosphorylation we measured the activity of endogenous PKA using the cytosolic FRET based A-kinase activity reporter AKAR3 (Allen and Zhang, 2006). As summarized in **Fig. 5A**, upon

challenge with forskolin 25 μM, cells over-expressing AKAR3 in combination with AKAP450-2 show a significantly higher cytosolic PKA activity than control cells expressing AKAR3 alone. No difference in PKA activity was observed when AKAR3 was co-expressed with the AKAP79 (**Fig. 5B**). To establish what is the functional outcome of having at the centrosome a microdomain with low cAMP concentration but a subset of PKA with higher sensitivity for cAMP, we used a variant of AKAR3 that includes the D/D domain at its amino terminus (RII_AKAR3) (Stangherlin et al., 2011) and therefore localizes at the centrosome (**Fig. 5C**). We found that RII_AKAR3 detects a higher PKA activity at the centrosome both in resting conditions (**Fig. 5D**) and in response to forskolin stimulation (**Fig. 5E**). The above results confirm that anchoring of PKA to AKAP450 lowers the activation threshold of PKA resulting in increased PKA activity at a given cAMP concentration and show that in interphase cells the low cAMP concentration at the centrosome is sufficient to maintain a higher basal phosphorylation activity of AKAP450-anchored PKA.

Anchoring of PKA to AKAP450 enhances RII subunit auto-phosphorylation. It is well established that auto-phosphorylation of the RII subunit at Ser114 (Kim et al., 2006) results in a reduced activation threshold for PKA (Taylor et al., 1990; Taylor et al., 2008). We therefore asked whether anchoring of PKA to AKAP450 may favor auto-phosphorylation of RII at S114. As shown in **Fig. 6A-B** we found that phosphorylation at S114 of both endogenous RII subunits and over-expressed recombinant RII-CFP subunits was indeed significantly increased in CHO cells over-expressing AKAP450-2. To further assess whether auto-phosphorylation of RII is the mechanism responsible for the higher sensitivity to cAMP displayed by the PKA subset anchored to AKAP450, we

generated a mutant of the PKA-GFP sensor (*mut*PKA-GFP) in which the RII subunit contains a S114A substitution, resulting in ablation of RII auto-phosphorylation (Rodriguez-Vilarrupla et al., 2005; Taylor et al., 1990; Wehrens et al., 2006) (**Fig. 6C**). When *mut*PKA-GFP was over-expressed in combination with AKAP450-2 and FRET changes measured in the bulk cytosol, the FRET change in response to 25 μM forskolin was of the same amplitude as the change measured in cells expressing the mutant sensor alone (**Fig. 6D**) indicating that auto-phosphorylation at S114 is necessary for the ability of AKAP450-2 to affect the activation threshold of PKA. *mut*PKA-GFP maintains an intact D/D domain and can therefore anchor to the centrosome (**Fig. 6E, insert**). When CHO cells expressing *mut*PKA-GFP were challenged with 25 μM forskolin and the FRET change measured in the cytosol and at the centrosome in the same cell, we found no significant difference between the two compartments (**Fig. 6E**), confirming that the higher sensitivity to cAMP of the centrosome-anchored PKA requires auto-phosphorylation of RII at S114.

The centrosomal microdomain with low cAMP is abrogated in mitosis. To investigate the possible functional relevance of the centrosomal microdomain with low cAMP we sought to establish whether the difference between cytosolic and centrosomal cAMP levels changes in different stages of the cell cycle. As shown in **Fig. 7A,** mitotic cells expressing RII_Epac show a uniform cAMP level at the centrosome and in the bulk cytosol. The global cAMP concentration in mitotic cells does not appear to be significantly different from the global cAMP concentration in interphase cells (**Fig. 7B**), indicating that a selective increase in cAMP concentration occurs at the centrosome site in mitosis. Notably, in agreement with the local increase in cAMP concentration at the

centrosome in mitotic cells, PKA phosphorylation activity is further increased selectively at this site, as detected by the RII_AKAR3 reporter (compare **Fig. 7C** and **Fig 5C-D**, 3.98%±0.57 and 6.69%±0.4 higher FRET signal in the centrosome compared to the cytosol in interphase and mitosis, respectively, p=0.0005). The above data indicate that the centrosomal cAMP microdomain is dynamic and is abrogated in mitotic cells.

As the MAP kinase ERK has been shown to inhibit PDE4D3 via phosphorylation of its catalytic domain (Baillie et al., 2000) we asked whether mitogenic stimuli that activate the MAP kinase pathway could affect the centrosomal cAMP microdomain. As shown in **Fig. 7D** in CHO cells stably expressing RII_Epac and treated with 10 nM EGF the centrosomal microdomain with low cAMP was completely abrogated as a consequence of a selective increase of the FRET signal at this site.

Local manipulation of cAMP signals at the centrosome distinctly affects the cell cycle. It has been previously reported that displacement of the endogenous centrosomal AKAP450 and the consequent delocalization of centrosomal PKA type II impairs cell cycle progression (Keryer et al., 2003), indicating that centrosomal PKA may play an important role in the control of cell division. The data presented above suggest that the unique handling of cAMP signals at the centrosome at different stages of the cell cycle may be important for the regulation of cell cycle progression. To test this hypothesis we used flow cytometric analysis to monitor the effects on the cell cycle of displacing endogenous PDE4D3 with dnPDE4D3, a maneuver that results in local increase of cAMP at the centrosome (**Fig. 3J-K** and **Fig. 8E**). We found that CHO cells stably expressing dnPDE4D3 show a significantly higher number of cells in G_2/M and significantly lower number of cells in S phase, suggestive of a block of the cell cycle in

G_2/M (**Fig. 8A**). Similar results were found in cells synchronized in S phase prior to analysis (**Suppl. Fig. 5**). In contrast, and as previously described (Gutzkow et al., 2002), treatment of CHO cells with 25 μM forskolin, which ensues a global increase in cAMP levels (**Fig. 8E**), results in a block of the cell cycle in G_1, with an increased proportion of cells with 2N DNA content, a significantly reduced number of cells in S phase but no change in G_2/M (**Fig. 8B**). Over-expression of a catalytically inactive version of the control enzyme dnPDE4A4 did not show any effect on the cell cycle (**Fig. 8C**). Inhibition of all PDE4 isoforms with 10μM rolipram, a treatment that results in increase of cAMP both at the centrosome and in the cytosol, albeit at a lower level than elicited by forskolin (**Fig. 8E**), did not result in a detectable effect on cell cycle progression (**Fig. 8D**). The above findings show that selective local manipulation of cAMP at the centrosome activates a downstream pathway with distinct effects on cell division.

Ablation of the centrosomal microdomain with low cAMP results in accumulation of cells in prophase. In order to gain further insight into the mechanism responsible for accumulation of cells in G_2/M when the centrosomal cAMP microdomain is perturbed, we generated a stable CHO cell clone expressing a RFP-tagged histone 2B (H2B-RFP) alone or in combination with a GFP-tagged dnPDE4D3 or dnPDE4A4. H2B-RFP labels the chromatin and allows for identification of different phases of the cell cycle. As illustrated in **Fig. 9A**, interphase cells show a homogeneous red fluorescence in the nucleus; cells in prophase can be clearly identified by the presence of condensed chromatin and an intact nuclear membrane; subsequent mitotic phases can be identified by the position of the chromosomes along the mitotic fuse. Using this approach we

assigned cells to one of the following categories: interphase, prophase, metaphase, anaphase/telophase. We found that CHO cells co-expressing H2B-RFP and dnPDE4D3 have a significantly higher number of cells in prophase compared to CHO cells expressing H2B-RFP alone or H2B-RFP in combination with dnPDE4A4 (**Fig. 9B**).

Discussion

The data reported here strongly support the novel proposal that: i) the centrosome in interphase is a subcellular compartment in which basal cAMP levels are lower than in the bulk cytosol as a consequence of centrosomal localization of PDE4D3; ii) anchoring of PKA to centrosomal AKAP450 lowers the activation threshold of PKA as a consequence of increased auto-phosphorylation of AKAP450-anchored RII subunits at S114; iii) the centrosomal cAMP microdomain is dynamic and is abrogated in mitosis, possibly via activation of the MAP kinase pathway; iv) manipulation of cAMP at the centrosome via displacement of PDE4D3 uniquely affects cell cycle progression resulting in a highly significant increase in the number of cells in G_2/M phase with accumulation of cells selectively in prophase. These findings demonstrate that local regulation of cAMP signals at the centrosome is critical for control of cell division.

In addition to a well established function as microtubule organizing centre, the centrosome has recently been shown to play a role in cell cycle control (Doxsey et al., 2005). For example, active maturation promoting factor (MPF), the key initiator of mitosis, is found at the centrosome during prophase (Jackman et al., 2003) and studies in which the centrosome was removed by microsurgical dissection (Hinchcliffe et al., 2001) or laser ablation (Khodjakov and Rieder, 2001) have provided direct evidence for a role of the centrosome in cell cycle progression. Of particular note, cell cycle arrest in G_1 (Gillingham and Munro, 2000; Keryer et al., 2003), as well as a block of cytokinesis (Keryer et al., 2003), were observed when AKAP450 and PKA were selectively displaced from the centrosome, suggesting that a cAMP/PKA signaling module localized at this site may serve a critical role. cAMP/PKA signaling has been shown to

be involved in many aspects of cell cycle regulation, including centrosome duplication, S-phase, G_2 arrest, mitotic spindle formation, exit from M-phase and cytokinesis (Matyakhina et al., 2002) and it is possible that different cAMP/PKA signaling modules may be responsible for the regulation of specific cell cycle-related events. In line with this view, our results show that whereas a global increase in cAMP levels, as generated by forskolin stimulation, results in an accumulation of cells in G_1, the local increase of cAMP generated by displacing PDE4D3 from the centrosome has a completely different effect, resulting in accumulation of cells in G_2/M. Further investigations will be necessary to identify the specific targets downstream of AKAP450-anchored PKA. However, in agreement with our findings, cAMP/PKA-dependent reduction of histone H3 phosphorylation (Rodriguez-Collazo et al., 2008b), an event that results in disruption of G_2 progression in adenocarcinoma cells, has been shown to require a concentration of cAMP that is significantly lower than the amount of cAMP necessary for PKA-mediated phosphorylation of CREB (Rodriguez-Collazo et al., 2008a), suggesting that the pool of PKA responsible for control of G_2 progression is more sensitive to cAMP than the pool of PKA that regulates gene transcription.

The data reported here clearly show that cAMP signals are uniquely processed at the centrosome where a high-sensitivity PKA subset is associated with a PKA-activatable and ERK-inhibitable PDE. Our findings are compatible with a model whereby the lower activation threshold of PKA tethered to AKAP450 allows for local activation of PKA at a concentration of cAMP that is insufficient to activate PKA subsets at other subcellular locations. Mitogenic stimuli selectively increase cAMP at the centrosome resulting in further activation of PKA at this site in the absence of global increase of cAMP levels. In

agreement with this model, over-expression of a catalytically inactive mutant of PDE4D3 in COS1 cells was shown to result in its PKA-dependent hyper-phosphorylation selectively at the centrosome even at resting levels of cAMP (McCahill et al., 2005), suggesting that the centrosomal PDE4D3 modulates activation of the local pool of PKA at basal cAMP concentrations. The feed-back loop mechanism described here and involving a high-sensitivity subset of PKA coupled with a PKA-activatable and ERK-inhibitable PDE at the centrosome, not only allows tight temporal control of centrosomal cAMP signals, but also provides a potential basis for autonomous regulation of centrosomal cAMP/PKA-dependent events, independently of global increase in cAMP and therefore of G_s protein-coupled receptors activation.

The functional relevance of the centrosomal cAMP microdomain that we have identified is illustrated by the disruption of cell cycle progression in CHO cells in which cAMP levels are selectively elevated at the centrosome via over-expression of a catalytically inactive PDE4D3. We found that in these conditions cell cycle progression is disrupted and cells accumulate in prophase. Of note, we also found that over-expression of dnPDE4D3 is not tolerated in RPE1 cells (**Suppl. Fig 3**), indicating that the effect of manipulating the centrosomal cAMP microdomain may be incompatible with cell cycle progression in non-transformed cells.

The data presented here show that during interphase, although the cAMP level at the centrosome is lower than in the bulk cytosol, it is sufficient to maintain a tonic activity of PKA at this site as a consequence of the reduced activation threshold of the local PKA subset. This finding is in agreement with the established notion that PKA activity is required to maintain cells in interphase (Bombik and Burger, 1973); (Lamb et al., 1991).

Our analysis shows that in mitosis there is a further increase in PKA activity at the centrosome, raising the question of how PKA activity is tuned temporally to allow progression from interphase to mitosis. Further studies with higher temporal resolution will be necessary to dissect cAMP signals and PKA activity at the centrosome within the same cell as it progresses from interphase and through mitosis in order to establish whether there is a short temporal window within which PKA activity is reduced to allow the interphase/mitosis transition. In this context, the activity of phosphatases may also be critical as it may counterbalance substrate phosphorylation by a tonically active centrosomal PKA subset.

Our study uncovers a completely novel mechanism of PKA activity regulation. Such regulation relies on binding of PKA to AKAP450 and the consequent reduction of the kinase activation threshold rather than on changes in the level of cAMP and is therefore effective only at the sites where AKAP450 is localized. Non-centrosomal splice variants of AKAP450 localize at the sarcolemma of cardiac myocytes in a complex with the slowly activating potassium channels I_{Ks} (Walsh and Kass, 1988) and to NR1 subunits of glutamate receptors at post-synaptic sites in neurons (Lin et al., 1998) and it will be interesting to establish whether the regulation described here at the centrosome also operates at these other sites. The novel mechanism we describe defines a new function for AKAPs and introduces a further level of complexity to the already sophisticated regulation of cAMP/PKA signaling and may have implications that extend beyond the control of cell cycle progression.

Material and Methods

Reagent

Forskolin (cat. n°F6886), Rolipram (cat. n°R6526), Cilostamide (cat. n°C7971), EHNA (cat. n°E114), H-89 (cat. n°B1427), EGF (cat. n°E9644) were purchased from SIGMA.

Generation of fluorescent chimeras

The CFP tagged R subunit of PKA (Lissandron et al., 2005) was sub-cloned into pCDNA3.1/Zeo (+) as a NheI/XbaI fragment. For the generation of *mut*RII-CFP the S114A mutation was introduced using the QuickChange™ Site-directed Mutagenesis Kit (cat. n°200518, Stratagene). The AKAP450-2 fragment from amino acid 933 to amino acid 1804 encoded by the AKAP450 cDNA (DDBJ/EMBL/GenBank accession N°AJ131693) (Witczak et al., 1999) was amplified by PCR and sub-cloned as a NheI/BamHI fragment in pcDNA3.1/Hygro (+). For *mut*AKAP450-2 the S1451P mutation was introduced using the QuickChange™ Site-directed Mutagenesis kit. The Rt31 fragment from amino acid 2 to amino acid 1678 (DDBJ/EMBL/GenBank accession N°AF387102) (Klussmann et al., 2001) was PCR amplified and sub-cloned as an EcoRI/XhoI insert into pIRES vector (cat. n°631605, Clontech). Generation of dnPDE4D3mRFP: the sequence encoding for dnPDE4D3 (McCahill et al., 2005) was amplified by PCR and sub-cloned into the BstXI site of the multiple cloning site of pcDNA3.1/Hygro (+). The monomeric red fluorescent protein was then inserted as XhoI/XbaI fragment in frame at the C-terminus of dnPDE4D3. A schematic of the sensors and AKAP fragments used in this study is shown in **Suppl. Fig. 2.**

Cell culture and transfection

CHO-K1 cells from Hamster Chinese ovary (Puck et al., 1958) were grown in Ham's F-12 medium (cat. n°21765-029, Invitrogen) supplemented with 10% (v/v) FBS (cat. n°10270106, Invitrogen), 2 mM L-glutamine (cat. n°25030-024, Invitrogen), 100 U/ml penicillin and 100 µg/ml streptomycin (cat. n°P07081, SIGMA) at 37°C in a humidified atmosphere containing 5% CO_2. SH-SY5Y cells from human neuroblastoma (Biedler et al., 1978) were grown in Ham's F-12:EMEM (cat. n°42430-025, Invitrogen) (1:1) supplemented with 10% (v/v) FBS, 2 mM L-glutamine, 1% (v/v) non essential amino acids (cat. n°11140-035, Invitrogen), 100 U/ml penicillin and 100 µg/ml streptomycin at 37°C in a humidified atmosphere containing 5% CO_2. RAW 264.7 cells (Raschke et al., 1978) were grown in Dulbecco's Modified Eagle Medium (DMEM) (cat. n°41966, Invitrogen) supplemented with 10% (v/v) FBS (cat. n° F9665, SIGMA), 2 mM of L-glutamine, 100 U/ml of penicillin and 100 µg/ml streptomycin at 37°C in a humidified atmosphere containing 5% CO_2. Enriched primary cultured of neonatal ventricular heart fibroblasts (RCF) were obtained from 1- to 3-day old Sprague Dawley rats as described in (Mongillo et al., 2006) . Briefly rats were killed by cervical dislocation and ventricular tissue was enzymatically digested with a mixture of collagenase (Roche) and pancreatin (Sigma). The isolated cell suspension was pre- plated for 2 hours in DMEM high glucose (cat. n°42430025, Invitrogen) supplemented with 20% (v/v) M-199 (cat. n°31150022, Invitrogen), 5% (v/v) horse serum, 0.5% (v/v) new born calf serum, 2 mM of L-glutamine, 10 U/ml of penicillin and 10 µg/ml streptomycin at 37°C in a humidified atmosphere containing 5% CO_2. The plastic-adherent non-myocyte cells obtained are fibroblasts. These were trypsinized and plated on coverslips for further analysis. Human Olfactory Neurons (HON) were grown in DMEM/F12 (cat. n°11330-032, Invitrogen)

supplemented with 10% (v/v) FBS, 100 U/ml penicillin and 100 µg/ml streptomycin at 37°C in a humidified atmosphere containing 5% CO_2. The retinal pigment epithelial RPE1 cells (Bodnar et al., 1998) were grown in DMEM:F-12 medium (cat. n° 11320-074, Invitrogen) supplemented with 10% (v/v) FBS (cat. n°10270106, Invitrogen), 2 mM L-glutamine (cat. n°25030-024, Invitrogen), 100 U/ml penicillin and 100 µg/ml streptomycin (cat. n°P07081, SIGMA) at 37°C in a humidified atmosphere containing 5% CO_2.

For transient expression, cells were seeded onto 24-mm glass coverslips in complete medium and grown for 24 hours as described in (Terrin et al., 2006). Transfections were performed at 50–70% of confluence. All cell types were transfected with TransIT®-LT1 Reagent (cat. n°M2300, Mirus) following the supplier's instructions and using 2-4 µg of DNA per coverslip. Experiments were performed 24-48 hours after transfection.

Knock down of PDE4D was achieved by using a small interfering RNA oligonucleotide targeting the PDE4D gene (125nM final concentration) (sequence: GAACUUGCCUUGAUGUACA, Thermo scientific Dharmacon) as previously described (Lynch et al., 2005). Control experiments were carried out using siGLO® Red transfection indicator (125 nM) (cat. n°D-001630-02-20, Thermo scientific Dharmacon).

Generation of stable clones

Stable clones expressing the PKA-GFP sensor have been described before (Vaasa et al., 2010). Briefly a CHO clones stable expressing RII-CFP was selected with 300 µg/ml of Zeocine™ and successively used to select a stable clones expressing the C-YFP

subunit by using 800 µg/ml of Geneticin®; CHO clones stably expressing either RII_epac or RII_AKAR3 sensor (Di Benedetto et al., 2008) were obtained by selection with 800 µg/ml of Geneticin®; CHO and RPE1 clones stably expressing dnPDE4D3mRFP1 were selected using 700 µg/ml of Hygromycin B (Invitrogen); CHO stable clone expressing pcDNA3dnPDE4A4-GFP was selected using 800 µg/ml of Geneticin® (Promega). Stable clones expressing either the GFP- or the RFP- tagged histone H2B were obtain by selection with 5 µg/ml of Blasticidin S (Invitrogen). In all cases, after 12 days treatment with the antibiotic cells were seeded in a 96 plate at 0.8 cells/well and single clones growing in individual wells selected for further expansion.

RT-PCR

Total mRNA was extracted with TRIzol® Reagent (cat. n°15596026, Invitrogen) from cells transfected with dnPDE4D3mRFP before or after selection with Geneticin. An aliquot of total mRNA was reversed transcribed with 1 µl SuperScript™ II RT 2000U/µl (cat. n 18064022, Invitrogen) to generate cDNA. Amplification of the coding regions of dnPDE4D3mRFP was performed by using specific primers annealing on the D484A mutation (McCahill et al., 2005). Primers used were as follows: 5'-GGTAACCGGCCCTTGACTG-3' and 5'-GGTTCTTCAGAATATGGTGCACTGTGCAGAT-3' for amplification of PDE4D3 wild type; 5'-GGTAACCGGCCCTTGACTG-3' and 5'-GGTTCTTCAGAATATGGTGCACT GTGCAGCA-3' for amplification of dnPDE4D3.

FRET imaging

Cells stably or transiently expressing a FRET-based cAMP sensor were imaged 24 hours after transfection as described in (Monterisi et al., 2012). Briefly, cells were imaged on an Olympus IX81 inverted microscope equipped with a PlanApoN 60X/1.42 oil immersion objective, an ORCA AG CCD camera (Hamamatsu) and a custom made beam splitter including the specific set of emission filters for CFP and YFP acquisition (dichroic mirror 505DCLP, YFP emission 545 nm, CFP emission 480 nm, Chroma Technology). During FRET experiments cells were bathed with 37°C pre-warmed PBS. Images were acquired using CellR software (Olympus) and processed using ImageJ (National Institutes of Health, Bethesda). FRET changes were measured in different cell compartments by drawing a region of interest (ROI) around a specific compartment (centrosome or cytosol). FRET changes of all the cAMP sensors were measured as changes in the 480/545-nm fluorescence emission intensities after background subtraction on excitation at 430 nm. For AKAR3 and RII_AKAR3 sensors FRET changes were measured as changes in the ratio between 545/480-nm fluorescent emission intensities after background subtraction upon excitation at 430nm. For dynamic FRET changes: the kinetic of the 480/545-nm emission intensity ratio is plotted against time and the average FRET response is expressed as % $\Delta R/R_0$, where $\Delta R = R - R_0$, R_0 is the ratio at time = 0 seconds (s) and R is the ratio at time = t seconds (s). For steady-state (or basal) FRET: 480/545-nm emission intensity values measured in the cytosol (R_{cyt}) and at the centrosome (R_{centr}) are expressed as normalized values with respect to the basal FRET ratio value measured in the cytosol (R_{cyt}). Ratio-metric images are displayed in pseudo-color, according to a user-defined lookup table that assigns a different color to each ratio value, as indicated.

Western Blotting and immunoprecipitation

Untransfected CHO cells or CHO cells stably expressing PKA-GFP were seeded on 10 cm tissue culture dishes, treated as indicated and washed twice with ice cold D-PBS before cell lysis. Cell lysates were prepared in lysis buffer containing 25 mM Hepes, pH 7.5, 2.5 mM EDTA, 50 mM NaCl, 30 mM sodium pyrophosphate, 10% (v/v) glycerol and 1% (v/v) Triton X-100 (cat. n°106K0177, SIGMA) and Complete™ EDTA-free protease inhibitor cocktail tablets (cat. n°11836170001, Roche). AKAP450-GFP was isolated from cells lysates via immunoprecipitation with GFP-trap beads (cat. n°gta-100, Chromotec) following the manufacturer's instructions. Protein concentration was determined using the Bradford Protein Assay (Biorad). Proteins were separated by gradient gel electrophoresis on NuPAGE Novex 4-12% Bis-Tris gels (Invitrogen) and transferred to Polyvinylidene fluoride (PVDF) membranes (Millipore). Membranes were then blocked either with Protein-Free T20 (TBS) Blocking Buffer (Thermo Scientific) or 5% (w/v) skimmed milk in TBS-T for 1 hour at room temperature. The following antibodies were used to probe the membranes: Mouse Anti-PKA_{RII} (BD Transduction Laboratories™), Mouse Anti-PKA_{RII} (pS114) (BD Transduction Laboratories™), goat pan-PDE4D (kind gift from Prof Miles Houslay, University of Glasgow) and goat Anti γ-tubulin (C-20) (Santa Cruz). Results, representing the mean of at least three independent experiments, were normalized to the amount of γ-tubulin.

Cells synchronization

G_1/S synchrony was obtained by double block with thymidine (Sigma). Briefly cells were treated with 5 mM thymidine in FBS-free medium for 16 hours, released to cycle in

medium supplemented with FBS for 8 hours and blocked again for additional 16 hours. Cells were let to recover for 24 hours in completed medium with or without 10 µM rolipram before FACS analysis.

Immunostaining and Confocal Imaging

Cells, transiently or stably expressing the PKA-GFP sensor, were washed three times with ice cold D-PBS. The centrosome was exposed by treatment with PHEM solution (45 mM Pipes, 45 mM HEPES, 10 mM EGTA, 5 mM $MgCl_2$, 1 mM PMSF and 0.1% (v/v) Triton X-100, pH 6.9) for 30 seconds at room temperature. Cells were then fixed with ice cold methanol for 5 minutes at -20°C, washed twice in D-PBS and saturated in 3% BSA for 30 minutes at room temperature. Primary antibodies were diluted in 3% BSA and incubated overnight in a wet chamber. CTR453 (Bailly et al., 1989) was used at a 1:5 dilution, rabbit anti-PDE4D3 (kind gift from Prof Miles Houslay, University of Glasgow, UK) was used at a 1:500 dilution and goat anti γ-tubulin (C-20) (Santa Cruz) was used at 1:2000. Goat anti-mouse AlexaFluor® 568 (Invitrogen), goat anti-rabbit AlexaFluor® 568 (Invitrogen) and donkey anti-goat AlexaFluor® 488 (Invitrogen) were used as secondary antibodies. Secondary antibody alone was used for controls. Confocal images were acquired with a Nikon Eclipse TE300 inverted microscope equipped with a spinning disk confocal system (Ultraview LCI; PerkinElmer), a 60×1.4 NA PlanApo objective (Nikon) and an Orca ER 12-bit CCD camera (Hamamatsu). Cells were excited at 568 nm laser line of a 643 series Argon-Krypton-Laser Melles Griot (643-Ryb-A02; Melles Griot) for imaging of the AlexaFluor568 fluorophore and the 405 nm line of a diode laser (iFlex2000; Point Source) for imaging CFP. The emission filters were 607/45 for the red emission and 480/30 for the cyan emission, respectively.

Flow cytometry scan analysis

Approximately 10^6 of cells were treated as indicated and grown in a T75 flask for 48 hours. After 48 hours exponentially growing cells were trypsinized, washed twice with D-PBS, and re-suspended in 300 μl of D-PBS. 700 μl of ice-cold 70% (v/v) EtOH/PBS was added drop-wise and the samples were incubated at 4°C for 1 hour. After incubation cells were spun down, washed with 1 ml of D-PBS, re-suspended in 250 μl of D-PBS containing 5 μl of 10 mg/ml RNAaseA (SIGMA) and incubated for 1 hour at 37°C. Samples were stained with 5 μl of 1 mg/ml of propidium iodide and kept in the dark at 4°C until analysis. Flow cytometric analysis was performed using a FACSCalibur flow cytometer (Becton Dickinson) and data collected were analyzed with FlowJo software and computed using the "Dean-Jett-Fox" model.

Statistics

Data are presented as mean ± standard error (SEM). Two tailed paired and un-paired Student's t-tests were used to determine significance between groups, as indicated. Number of replicates and the type of Student's t-test used are indicated in the text. Asterisks are used to indicate levels of significance based on p-values: * $p<0.05$; ** $0.001<p<0.01$; *** $p<0.001$.

Online supplementary material.

FigS1 shows that PKA-GFP localizes at the centrosome and that its over-expression does not affect the centrosome morphology. **Fig.S2** shows a schematic representation of the RII_epac sensor, AKAP450 and AKAP450-2 fragment. A schematic of the

interaction between the FRET-based sensors and AKAP constructs used in this study is also shown. **Fig. S3** shows the localization of the PKA-GFP sensor and PDE4D3 in the non-transformed cell line RPE1. Fig.S3 shows also analysis of the basal FRET signal at the centrosome and in the bulk cytosol in the same cell line. **Fig.S4** shows the localization of endogenous PDE4D3 in CHO cells, the efficiency of its knock-down and the localization of the over-expressed catalytically dead PDE4D3 isoform in CHO cells. **Fig.S5** shows the FACS analysis of cell cycle progression in CHO, CHO treated with rolipram and CHO stably expressiong the catalytically dead PDE4D3 after synchronization in G_1/S phase.

Acknowledgements

The authors would like to thank Miles Houslay (University of Glasgow) for dnPDE4D3, dnPDE4A4-GFP and goat anti pan-PDE4D and rabbit anti-PDE4D3 antibodies; John D. Scott (Howard Hughes Medical Institute, University of Washington) for SuperAKAP-IS-GFP; Kjetil Taskén, (University of Oslo) for AKAP450-2, AKAP79, AKAP149 and RIAD-GFP; Enno Klussmann, (Max-Delbrück-Centrum für Molekulare Medizin, Berlin) for Rt31; Jin Zhang, (Johns Hopkins Institute,Baltimore, USA) for AKAR3 and Guy Keryer (Institut Curie, Orsay) for the CTR453 AKAP450 specific antibody. This work was supported by the Fondation Leducq (O6 CVD 02), the British Heart Foundation (PG/07/091/23698) and the NSF-NIH CRCNS program (NIH R01 AA18060) to MZ.

Abbreviations List

aa = amino acid

AC = adenylyl cyclases

AKAP = A Kinase anchoring proteins

AKAR3 = A-Kinase activity reporter

cAMP = 3', 5' cyclic adenosine monophosphate

CFP = cyan fluorescent protein

CREB = CRE binding protein

D/D = docking domain

EHNA = erythro-9-2-hydroxy-3-nonyl adenine

ERK = extracellular regulation kinase

FACS = Flow cytometry scan analysis

FRET = fluorescence resonance energy transfer

GFP = green fluorescent protein

MPF = Maturation Promoting Factor

mRFP = monomeric ref fluorescent protein

PDE = phosphodiesterase

PKA = cAMP-dependent protein kinase

SEM = standard error of measurement or mean

YFP = yellow fluorescent protein

References

Allen, M.D., and J. Zhang. 2006. Subcellular dynamics of protein kinase A activity visualized by FRET-based reporters. *Biochem Biophys Res Commun*. 348:716-721.

Alto, N.M., S.H. Soderling, N. Hoshi, L.K. Langeberg, R. Fayos, P.A. Jennings, and J.D. Scott. 2003. Bioinformatic design of A-kinase anchoring protein-in silico: a potent and selective peptide antagonist of type II protein kinase A anchoring. *Proc Natl Acad Sci U S A*. 100:4445-4450.

Baillie, G.S., S.J. MacKenzie, I. McPhee, and M.D. Houslay. 2000. Sub-family selective actions in the ability of Erk2 MAP kinase to phosphorylate and regulate the activity of PDE4 cyclic AMP-specific phosphodiesterases. *Br J Pharmacol*. 131:811-819.

Bailly, E., M. Doree, P. Nurse, and M. Bornens. 1989. p34cdc2 is located in both nucleus and cytoplasm; part is centrosomally associated at G2/M and enters vesicles at anaphase. *Embo J*. 8:3985-3995.

Biedler, J.L., S. Roffler-Tarlov, M. Schachner, and L.S. Freedman. 1978. Multiple neurotransmitter synthesis by human neuroblastoma cell lines and clones. *Cancer Res*. 38:3751-3757.

Bodnar, A.G., M. Ouellette, M. Frolkis, S.E. Holt, C.P. Chiu, G.B. Morin, C.B. Harley, J.W. Shay, S. Lichtsteiner, and W.E. Wright. 1998. Extension of life-span by introduction of telomerase into normal human cells. *Science*. 279:349-352.

Bombik, B.M., and M.M. Burger. 1973. c-AMP and the cell cycle: inhibition of growth stimulation. *Exp Cell Res*. 80:88-94.

Carlson, C.R., B. Lygren, T. Berge, N. Hoshi, W. Wong, K. Tasken, and J.D. Scott. 2006. Delineation of type I protein kinase A-selective signaling events using an RI anchoring disruptor. *J Biol Chem*. 281:21535-21545.

Carlson, C.R., A. Ruppelt, and K. Tasken. 2003. A kinase anchoring protein (AKAP) interaction and dimerization of the RIalpha and RIbeta regulatory subunits of protein kinase a in vivo by the yeast two hybrid system. *J Mol Biol*. 327:609-618.

Conti, M., and J. Beavo. 2007. Biochemistry and physiology of cyclic nucleotide phosphodiesterases: essential components in cyclic nucleotide signaling. *Annu Rev Biochem*. 76:481-511.

Cuschieri, L., T. Nguyen, and J. Vogel. 2007. Control at the cell center: the role of spindle poles in cytoskeletal organization and cell cycle regulation. *Cell Cycle*. 6:2788-2794.

Di Benedetto, G., A. Zoccarato, V. Lissandron, A. Terrin, X. Li, M.D. Houslay, G.S. Baillie, and M. Zaccolo. 2008. Protein kinase A type I and type II define distinct intracellular signaling compartments. *Circ Res*. 103:836-844.

Dodge, K.L., S. Khouangsathiene, M.S. Kapiloff, R. Mouton, E.V. Hill, M.D. Houslay, L.K. Langeberg, and J.D. Scott. 2001. mAKAP assembles a protein kinase A/PDE4 phosphodiesterase cAMP signaling module. *Embo J*. 20:1921-1930.

Doxsey, S., W. Zimmerman, and K. Mikule. 2005. Centrosome control of the cell cycle. *Trends Cell Biol*. 15:303-311.

Feliciello, A., M.E. Gottesman, and E.V. Avvedimento. 2001. The biological functions of A-kinase anchor proteins. *J Mol Biol*. 308:99-114.

Gillingham, A.K., and S. Munro. 2000. The PACT domain, a conserved centrosomal targeting motif in the coiled-coil proteins AKAP450 and pericentrin. *EMBO Rep*. 1:524-529.

Gold, M.G., B. Lygren, P. Dokurno, N. Hoshi, G. McConnachie, K. Tasken, C.R. Carlson, J.D. Scott, and D. Barford. 2006. Molecular basis of AKAP specificity for PKA regulatory subunits. *Mol Cell*. 24:383-395.

Gutzkow, K.B., S. Naderi, and H.K. Blomhoff. 2002. Forskolin-mediated G1 arrest in acute lymphoblastic leukaemia cells: phosphorylated pRB sequesters E2Fs. *J Cell Sci*. 115:1073-1082.

Herberg, F.W., A. Maleszka, T. Eide, L. Vossebein, and K. Tasken. 2000. Analysis of A-kinase anchoring protein (AKAP) interaction with protein kinase A (PKA) regulatory subunits: PKA isoform specificity in AKAP binding. *J Mol Biol*. 298:329-339.

Hinchcliffe, E.H., F.J. Miller, M. Cham, A. Khodjakov, and G. Sluder. 2001. Requirement of a centrosomal activity for cell cycle progression through G1 into S phase. *Science*. 291:1547-1550.

Houslay, M.D. 2010. Underpinning compartmentalised cAMP signalling through targeted cAMP breakdown. *Trends Biochem Sci*. 35:91-100.

Jackman, M., C. Lindon, E.A. Nigg, and J. Pines. 2003. Active cyclin B1-Cdk1 first appears on centrosomes in prophase. *Nat Cell Biol*. 5:143-148.

Keryer, G., O. Witczak, A. Delouvee, W.A. Kemmner, D. Rouillard, K. Tasken, and M. Bornens. 2003. Dissociating the centrosomal matrix protein AKAP450 from centrioles impairs centriole duplication and cell cycle progression. *Mol Biol Cell*. 14:2436-2446.

Khodjakov, A., and C.L. Rieder. 2001. Centrosomes enhance the fidelity of cytokinesis in vertebrates and are required for cell cycle progression. *J Cell Biol*. 153:237-242.

Kim, C., D. Vigil, G. Anand, and S.S. Taylor. 2006. Structure and dynamics of PKA signaling proteins. *Eur J Cell Biol*. 85:651-654.

Klussmann, E., B. Edemir, B. Pepperle, G. Tamma, V. Henn, E. Klauschenz, C. Hundsrucker, K. Maric, and W. Rosenthal. 2001. Ht31: the first protein kinase A anchoring protein to integrate protein kinase A and Rho signaling. *FEBS Lett*. 507:264-268.

Lamb, N.J., J.C. Cavadore, J.C. Labbe, R.A. Maurer, and A. Fernandez. 1991. Inhibition of cAMP-dependent protein kinase plays a key role in the induction of mitosis and nuclear envelope breakdown in mammalian cells. *Embo J*. 10:1523-1533.

Lin, J.W., M. Wyszynski, R. Madhavan, R. Sealock, J.U. Kim, and M. Sheng. 1998. Yotiao, a novel protein of neuromuscular junction and brain that interacts with specific splice variants of NMDA receptor subunit NR1. *J Neurosci*. 18:2017-2027.

Lissandron, V., A. Terrin, M. Collini, L. D'Alfonso, G. Chirico, S. Pantano, and M. Zaccolo. 2005. Improvement of a FRET-based indicator for cAMP by linker design and stabilization of donor-acceptor interaction. *J Mol Biol*. 354:546-555.

Lynch, M.J., G.S. Baillie, A. Mohamed, X. Li, C. Maisonneuve, E. Klussmann, G. van Heeke, and M.D. Houslay. 2005. RNA silencing identifies PDE4D5 as the functionally relevant cAMP phosphodiesterase interacting with beta arrestin to

control the protein kinase A/AKAP79-mediated switching of the beta2-adrenergic receptor to activation of ERK in HEK293B2 cells. *J Biol Chem*. 280:33178-33189.

MacKenzie, S.J., G.S. Baillie, I. McPhee, C. MacKenzie, R. Seamons, T. McSorley, J. Millen, M.B. Beard, G. van Heeke, and M.D. Houslay. 2002. Long PDE4 cAMP specific phosphodiesterases are activated by protein kinase A-mediated phosphorylation of a single serine residue in Upstream Conserved Region 1 (UCR1). *Br J Pharmacol*. 136:421-433.

Matyakhina, L., S.M. Lenherr, and C.A. Stratakis. 2002. Protein kinase A and chromosomal stability. *Ann N Y Acad Sci*. 968:148-157.

McCahill, A., T. McSorley, E. Huston, E.V. Hill, M.J. Lynch, I. Gall, G. Keryer, B. Lygren, K. Tasken, G. van Heeke, and M.D. Houslay. 2005. In resting COS1 cells a dominant negative approach shows that specific, anchored PDE4 cAMP phosphodiesterase isoforms gate the activation, by basal cyclic AMP production, of AKAP-tethered protein kinase A type II located in the centrosomal region. *Cell Signal*. 17:1158-1173.

Mongillo, M., T. McSorley, S. Evellin, A. Sood, V. Lissandron, A. Terrin, E. Huston, A. Hannawacker, M.J. Lohse, T. Pozzan, M.D. Houslay, and M. Zaccolo. 2004. Fluorescence resonance energy transfer-based analysis of cAMP dynamics in live neonatal rat cardiac myocytes reveals distinct functions of compartmentalized phosphodiesterases. *Circ Res*. 95:67-75.

Mongillo, M., C.G. Tocchetti, A. Terrin, V. Lissandron, Y.F. Cheung, W.R. Dostmann, T. Pozzan, D.A. Kass, N. Paolocci, M.D. Houslay, and M. Zaccolo. 2006. Compartmentalized phosphodiesterase-2 activity blunts beta-adrenergic cardiac inotropy via an NO/cGMP-dependent pathway. *Circ Res*. 98:226-234.

Monterisi, S., M. Favia, L. Guerra, R.A. Cardone, D. Marzulli, S.J. Reshkin, V. Casavola, and M. Zaccolo. 2012. CFTR regulation in human airway epithelial cells requires integrity of the actin cytoskeleton and compartmentalized cAMP and PKA activity. *J Cell Sci*. 125:1106-1117.

Puck, T.T., S.J. Cieciura, and A. Robinson. 1958. Genetics of somatic mammalian cells. III. Long-term cultivation of euploid cells from human and animal subjects. *J Exp Med*. 108:945-956.

Raschke, W.C., S. Baird, P. Ralph, and I. Nakoinz. 1978. Functional macrophage cell lines transformed by Abelson leukemia virus. *Cell*. 15:261-267.

Rodriguez-Collazo, P., S.K. Snyder, R.C. Chiffer, E.A. Bressler, T.C. Voss, E.P. Anderson, H.G. Genieser, and C.L. Smith. 2008a. cAMP signaling regulates histone H3 phosphorylation and mitotic entry through a disruption of G2 progression. *Exp Cell Res*. 314:2855-2869.

Rodriguez-Collazo, P., S.K. Snyder, R.C. Chiffer, J. Zlatanova, S.H. Leuba, and C.L. Smith. 2008b. cAMP signaling induces rapid loss of histone H3 phosphorylation in mammary adenocarcinoma-derived cell lines. *Exp Cell Res*. 314:1-10.

Rodriguez-Vilarrupla, A., M. Jaumot, N. Abella, N. Canela, S. Brun, C. Diaz, J.M. Estanyol, O. Bachs, and N. Agell. 2005. Binding of calmodulin to the carboxy-terminal region of p21 induces nuclear accumulation via inhibition of protein kinase C-mediated phosphorylation of Ser153. *Mol Cell Biol*. 25:7364-7374.

Schmidt, P.H., D.T. Dransfield, J.O. Claudio, R.G. Hawley, K.W. Trotter, S.L. Milgram, and J.R. Goldenring. 1999. AKAP350, a multiply spliced protein kinase A-anchoring protein associated with centrosomes. *J Biol Chem*. 274:3055-3066.

Sette, C., and M. Conti. 1996. Phosphorylation and activation of a cAMP-specific phosphodiesterase by the cAMP-dependent protein kinase. Involvement of serine 54 in the enzyme activation. *J Biol Chem*. 271:16526-16534.

Stangherlin, A., F. Gesellchen, A. Zoccarato, A. Terrin, L.A. Fields, M. Berrera, N.C. Surdo, M.A. Craig, G. Smith, G. Hamilton, and M. Zaccolo. 2011. cGMP signals modulate cAMP levels in a compartment-specific manner to regulate catecholamine-dependent signaling in cardiac myocytes. *Circ Res*. 108:929-939.

Stefan, E., B. Wiesner, G.S. Baillie, R. Mollajew, V. Henn, D. Lorenz, J. Furkert, K. Santamaria, P. Nedvetsky, C. Hundsrucker, M. Beyermann, E. Krause, P. Pohl, I. Gall, A.N. MacIntyre, S. Bachmann, M.D. Houslay, W. Rosenthal, and E. Klussmann. 2007. Compartmentalization of cAMP-dependent signaling by phosphodiesterase-4D is involved in the regulation of vasopressin-mediated water reabsorption in renal principal cells. *J Am Soc Nephrol*. 18:199-212.

Stork, P.J., and J.M. Schmitt. 2002. Crosstalk between cAMP and MAP kinase signaling in the regulation of cell proliferation. *Trends Cell Biol*. 12:258-266.

Takahashi, M., H. Shibata, M. Shimakawa, M. Miyamoto, H. Mukai, and Y. Ono. 1999. Characterization of a novel giant scaffolding protein, CG-NAP, that anchors multiple signaling enzymes to centrosome and the golgi apparatus. *J Biol Chem*. 274:17267-17274.

Tasken, K.A., P. Collas, W.A. Kemmner, O. Witczak, M. Conti, and K. Tasken. 2001. Phosphodiesterase 4D and protein kinase a type II constitute a signaling unit in the centrosomal area. *J Biol Chem*. 276:21999-22002.

Taylor, S.S., J.A. Buechler, and W. Yonemoto. 1990. cAMP-dependent protein kinase: framework for a diverse family of regulatory enzymes. *Annu Rev Biochem*. 59:971-1005.

Taylor, S.S., C. Kim, C.Y. Cheng, S.H. Brown, J. Wu, and N. Kannan. 2008. Signaling through cAMP and cAMP-dependent protein kinase: diverse strategies for drug design. *Biochim Biophys Acta*. 1784:16-26.

Terrin, A., G. Di Benedetto, V. Pertegato, Y.F. Cheung, G. Baillie, M.J. Lynch, N. Elvassore, A. Prinz, F.W. Herberg, M.D. Houslay, and M. Zaccolo. 2006. PGE(1) stimulation of HEK293 cells generates multiple contiguous domains with different [cAMP]: role of compartmentalized phosphodiesterases. *J Cell Biol*. 175:441-451.

Vaasa, A., M. Lust, A. Terrin, A. Uri, and M. Zaccolo. 2010. Small-molecule FRET probes for protein kinase activity monitoring in living cells. *Biochem Biophys Res Commun*. 397:750-755.

Walsh, K.B., and R.S. Kass. 1988. Regulation of a heart potassium channel by protein kinase A and C. *Science*. 242:67-69.

Wehrens, X.H., S.E. Lehnart, S. Reiken, J.A. Vest, A. Wronska, and A.R. Marks. 2006. Ryanodine receptor/calcium release channel PKA phosphorylation: a critical mediator of heart failure progression. *Proc Natl Acad Sci U S A*. 103:511-518.

Witczak, O., B.S. Skalhegg, G. Keryer, M. Bornens, K. Tasken, T. Jahnsen, and S. Orstavik. 1999. Cloning and characterization of a cDNA encoding an A-kinase anchoring protein located in the centrosome, AKAP450. *Embo J*. 18:1858-1868.

Wong, W., and J.D. Scott. 2004. AKAP signalling complexes: focal points in space and time. *Nat Rev Mol Cell Biol*. 5:959-970.

Zaccolo, M. 2009. cAMP signal transduction in the heart: understanding spatial control for the development of novel therapeutic strategies. *Br J Pharmacol*. 158:50-60.

Zaccolo, M., F. De Giorgi, C.Y. Cho, L. Feng, T. Knapp, P.A. Negulescu, S.S. Taylor, R.Y. Tsien, and T. Pozzan. 2000. A genetically encoded, fluorescent indicator for cyclic AMP in living cells. *Nat Cell Biol*. 2:25-29.

Zaccolo, M., and T. Pozzan. 2002. Discrete microdomains with high concentration of cAMP in stimulated rat neonatal cardiac myocytes. *Science*. 295:1711-1715.

Figure legends

Figure 1. **The FRET sensor PKA-GFP localizes to the centrosome via binding to endogenous AKAPs. A)** Upper panel: Schematic representation of the cAMP sensor PKA-GFP. RII-CFP: PKA regulatory subunit type II (RII) fused to the cyan fluorescent protein (CFP). D/D indicates the dimerization/docking domain; IS indicates the catalytic inhibitory site and auto-phosphorylation site; domain A and domain B indicate the cAMP binding domain A and B, respectively. C-YFP: catalytic subunit of PKA (C) fused to the yellow fluorescent protein (YFP). The lower panel illustrates the interaction of PKA-GFP with an AKAP (in green) and its mechanism of activation upon binding of cAMP. The yellow and blue halos around YFP and CFP indicate fluorescence emission from the fluorophores upon excitation of CFP at 430nm. **B)** Subcellular distribution of the sensor in a CHO cells stably expressing PKA-GFP in interphase (left) and mitosis (right). White arrows point to the centrosome and one of the centrioles, respectively. **C)** CHO cells stably expressing PKA-GFP and immunostained with a γ-tubulin specific antibody (top panels) and with the AKAP450-specific antibody CTR453 (middle panels). A negative control (nc) in which the primary antibody is omitted is shown in the bottom panels. The signal from the C-YFP component of the sensor is not shown. **D)** CHO cells expressing SuperAKAP-IS-GFP (left upper panel) and RIAD-GFP (left lower panel) in combination with RII-RFP (upper and lower panel on the right). Size bars = 10μm.

Figure 2. **Basal cAMP in interphase cells is lower at the centrosome than in the cytosol. A)** CHO cell stably expressing the PKA-GFP sensor. The middle panel in gray

scale is the image acquired at 480nm upon excitation at 430nm and shows the subcellular distribution of the sensor. The signal generated by the C-YFP component of the PKA-GFP sensor is not shown. The FRET signal from the same cell, calculated as 480nm/540nm emission intensity ratio upon excitation at 430nm, is shown in pseudo-color. Panels on the left show a higher magnification of the centrosomal region. White arrows point to the centrosome. The panel on the right shows the average basal FRET signal measured in the bulk cytosol (cyt) and at the centrosome (centr) of cells stably expressing PKA-GFP. FRET values are the average calculated within a region of interest (ROI) drawn to include the entire cytosolic area or the centrosome, respectively (an example is provided in Fig 4 A, B) and are expressed relative to the FRET value measured in the cytosol. n= 34 **B)** CHO cells stably expressing the unimolecular sensor RII_epac. Description of panels is as in A). n= 31. **C)** Sensor distribution and FRET pseudo-color images of RAW264.7 cells, SH-SY5Y cells, primary human olfactory neurons (HON) and primary rat cardiac fibroblasts (RCF) expressing RII_epac. For each cell type bottom panels show the average FRET signal in the cytosol and at the centrosome calculated as described in A). n≥ 5. For all experiments, error bars represent SEM. Two tailed; paired t-test, ∗ $p<0.05$; ∗∗∗ $p<0.001$. Size bars = 10μm.

Figure 3. **The low cAMP compartment at the centrosome depends on centrosomal PDE4D3. A)** Sensor distribution and FRET pseudo-color image of a representative CHO cell stably expressing PKA-GFP and treated with 10 μM rolipram. Panels on the left are a magnification of the centrosomal region. **B)** Average basal FRET signal calculated in the cytosol and at the centrosome in CHO cells expressing PKA-GFP and

treated with the PDE4 inhibitor rolipram (10 μM). n = 44 **C)** Average basal FRET signal calculated in the cytosol and at the centrosome in CHO cells expressing RII_epac and treated with 10 μM rolipram. n = 25 **D)** Sensor distribution and FRET pseudo-color image of representative CHO cells stably expressing PKA-GFP and treated with the PDE2 inhibitor EHNA (10 μM) and **E)** average basal FRET signal calculated in the cytosol and at the centrosome in the same cells. n = 46 **F)** Average basal FRET signal calculated in the cytosol and at the centrosome of CHO cells stably expressing PKA-GFP and treated with the PDE3 inhibitor cilostamide (10 μM). n = 39 **G)** Sensor distribution and FRET pseudo-color image of a representative CHO cell stably expressing PKA-GFP and in which PDE4D isoforms have been knocked down by small interference RNA treatment. The average FRET signal in the cytosol and centrosome in these cells and in cells expressing the control sequence siGLO are shown in **H)** (n = 40) and **I)** (n = 40), respectively. **J)** Sensor distribution and FRET pseudo-color image of a representative CHO cell stably expressing PKA-GFP and a catalytically inactive mutant of PDE4D3 (dnPDE4D3); the average FRET signal in the cytosol and centrosome (n = 31) is shown in **K)**. **L)** Summary of the basal CFP/YFP ratio values recorded in the cytosol and at the centrosome of cells expressing a catalytically inactive mutant of PDE4A4 (n = 21). Error bar represents SEM. Two-tailed, paired t-test, ∗ $p<0.05$; ∗∗∗ $p<0.001$). Size bars = 10μm.

Figure 4. **PKA-GFP anchored to AKAP450 shows increased sensitivity to cAMP. A)** On the left CHO cell stably expressing the RII_epac sensor. Representative region of interest (ROI) within which the ratio values are averaged for ‘bulk cytosol’ (black line)

and centrosome (grey line) are shown. On the right: normalized average kinetics (n = 31) of FRET change induced by 25 μM forskolin (frsk) in CHO cells stably expressing RII_epac and recorded in the cytosol (cyt; black circles) and at the centrosome (centr; grey circles). **B)** Left panel: CHO cell stably expressing the PKA-GFP sensor. Right panel: normalized average kinetics of FRET change detected in response to 25 μM frsk in CHO cells stably expressing PKA-GFP and recorded in the cytosol and at the centrosome (n = 35). **C)** Distribution of the GFP-tagged AKAP450-2 fragment in a representative CHO cell. **D)** Western blot analysis of lysates from CHO cells over-expressing the GFP-tagged AKAP450-2 fragment. AKAP450-2 was immunoprecipitated using GFP-trap beads and the total lysate (L), the unbound fraction (NB) and the protein bound fraction (B) to the GFP-trap beads were immunoblotted with anti-RII antibody. Similar results were obtained in three independent experiments. **E)** Normalized average kinetics (n = 25) of FRET change induced by 25 μM forskolin (frsk) in CHO cells expressing PKA-GFP in the presence (open circles) or absence (full circles) of AKAP450-2. **F)** Dose-response curve of FRET change at different concentration of forskolin in CHO cells expressing PKA-GFP in the presence (open circles) or absence (full cycles) of AKAP450-2. For each concentration point n ≥ 10. **G)** FRET change induced by 25 μM forskolin in CHO cells expressing PKA-GFP in the presence or absence of AKAP450-2 fragment and SuperAKAP-IS; n ≥ 18 **H)** FRET change induced by 25 μM forskolin in CHO cells expressing the deletion mutant sensor ΔPKA-GFP in the presence or absence of AKAP450-2; n ≥ 23 **I)** FRET change induced by 25 μM forskolin in CHO cells expressing PKA-GFP in the presence or absence of the AKAP450-2 and *mut*AKAP450-2. n ≥ 14 **J)** FRET change induced by 25 μM forskolin in

CHO cells expressing the RII_epac sensor in the presence or absence of the AKAP450-2; n ≥ 34 **K)** FRET change induced by 25 μM forskolin in CHO cells expressing PKA-GFP in the presence or absence of AKAP79 fragment (amino acid 352 to 428); n ≥ 24 **L)** FRET change induced by 25 μM forskolin in CHO cells expressing PKA-GFP in the presence or absence of AKAP149 fragment (amino acid 284 to 385); n ≥ 24 **M)** FRET change induced by 25 μM forskolin in CHO cells expressing PKA-GFP in the presence or absence of the AKAP Rt31 fragment (amino acid 2 to 1678); n ≥ 17. Error bars are SEM. Two-tailed, un-paired t-test, ∗ $p<0.05$; ∗∗ $0.001<p<0.01$; ∗∗∗ $p<0.001$. Size bars = 10μm

Figure 5. **Binding of PKA to AKAP450-2 increases PKA activity. A)** FRET change measured in response to 25 μM forskolin in CHO cells expressing AKAR3 in the presence or absence of AKAP450-2. n = 53. **B)** FRET change measured in response to 25 μM forskolin in CHO cells expressing AKAR3 in the presence or absence of AKAP79 fragment. n = 14. Two tailed, paired t-test. **C)** Gray scale image acquired at 480nm upon excitation at 430nm and showing the subcellular distribution of the RII_AKAR3 sensor. The pseudo-color panel shows the FRET signal from the same cell, calculated as 540nm/480nm emission intensity ratio upon excitation at 430nm. Panels on the left show a higher magnification of the centrosomal region. Arrows point to the centrosome. **D)** Average of basal FRET signal measured in the bulk cytosol (cyt) and at the centrosome (centr) of cells stably expressing the RII_AKAR3 sensor. FRET values are expressed relative to the FRET value measured in the cytosol, n= 30. Two tailed, paired t-test. **E)** Average of FRET change elicited by 100nM forskolin in cells stably expressing

the RII_AKAR3 sensor and recorded in the cytosol and at the centrosome. Error bars represents SEM. Two tailed, un-paired t-test, ∗ $p<0.05$; ∗∗ $0.001<p<0.01$; ∗∗∗ $p<0.001$. Size bars = 10μm.

Figure 6. **AKAP450-bound PKA is more sensitive to cAMP activation as a result of increased auto-phosphorylation of RII. A)** Representative western blot analysis of total RII and phospho-RII subunits. Lysates from CHO cells over-expressing PKA-GFP in the presence or absence of AKAP450-2 were blotted and probed for phospho-RII (upper panel) and total RII (lower panel) using specific antibodies. 80kDa and 53kDa are the expected molecular weight for recombinant RII-CFP and endogenous RII subunit, respectively. **B)** Quantification of endogenous phospho-RII (gray columns) and recombinant phospho-RII-CFP (black columns). Data are the mean of 5 independent experiments. Two-tailed, un-paired t-test. **C)** Western blot analysis of lysates from CHO cells expressing the PKA-GFP sensor or a mutant sensor (*mut*PKA-GFP) containing a S114A mutation in the RII-CFP subunit. Total and phosphor-RII subunits are detected as in A). **D)** FRET changes induced by 25 μM forskolin in CHO cells expressing PKA-GFP (black columns) and *mut*PKA-GFP (white columns) in the presence or absence of the AKAP450-2 fragment. n = 28. Two-tailed, un-paired t-test. **E)** Effect of 25 μM forskolin on the FRET signal detected in the cytosol (cyt) and at the centrosome (centr) of CHO cells expressing PKA-GFP (black columns) or *mut*PKA-GFP (white columns). n = 16. Insert: distribution of *mut*PKA-GFP in a representative CHO cell. Arrow points to the centrosome. Error bars are SEM. Two tailed, paired t-test, ∗ $p<0.05$; ∗∗ $0.001<p<0.01$; ∗∗∗ $p<0.001$. Size bars = 10μm.

Figure 7. **The centrosomal microdomain with low cAMP is abrogated in mitosis. A)** Representative mitotic CHO cell stably expressing the RII_epac sensor. The gray scale image shows the subcellular distribution of the RII_epac sensor and the pseudo-color image shows the FRET signal from the same cell. Arrows point to one of the centrioles. The histogram on the right displays the average basal FRET signal measured in the bulk cytosol (cyt) and at the centrioles (centr) in n=30 cells. FRET values are expressed relative to the FRET value measured in the cytosol, **B)** Comparison of the FRET signal recorded in the bulk cytosol in interphase (I) and in mitotic (M) CHO cells stably expressing RII_epac. n = 30. Two tailed, un-paired t-test. **C)** Representative mitotic CHO cell stably expressing the RII_AKAR3 sensor. Panels are as described in A. n= 22. Two tailed, paired t-test. **D)** Average FRET change measured before and after treatment with 10nM EGF in serum depleted CHO cells stably expressing RII_epac. n=20. Error bars represent SEM. Two tailed, un-paired t-test, $*$ $p<0.05$; $***$ $p<0.001$. Size bars = 10μm.

Figure 8**. Displacement of PDE4D3 results in altered cell cycle progression. A)** Quantification of flow cytometry scan analysis of control CHO cells and CHO cells stably expressing the RFP-tagged and catalytic inactive mutant of PDE4D3 (dnPDE4D3mRFP). The same analysis was performed for CHO cells treated with 25μM forskolin (**B**) CHO cells stably expressing the catalytic inactive mutant of PDE4A4 (dnPDE4A4-GFP) (**C**) and CHO cells treated with 10 μM rolipram (**D**). Histograms indicate the mean percentages of cells in various phases of the cell cycle. Data are the mean of at least 6 independent experiments. Error bars are SEM. Two tailed, un-paired

t-test, ∗ p<0.05; ∗∗ 0.05<p<0.01; ∗∗∗ p<0.001. **E)** Effect of over-expression of dnPDE4D3mRFP, 10 μM rolipram (Rol), 25 μM forskolin (FRSK) and over-expression of dnPDE4A4-GFP on cytosolic (cyt) and centrosomal (centr) cAMP compared to untreated and unstimulated CHO control cells (CTRL). Two tailed, un-paired t-test, ∗ p<0.05; ∗∗∗ p<0.001

Figure 9. **Over-expression of dnPDE4D3 results in accumulation of cells in prophase. A)** Representative living CHO cells stably expressing dnPDE4A4RFP and the GFP-tagged H2B imaged in interphase and in different phases of the mitotic cycle as appearent from the analysis of chromosome condensation. **B)** Summary of the results of seven independent experiments in which multiple snapshots of living CHO cells expressing either GFP-tagged H2B and dnPDE4A4RFP or RFP-tagged H2B and dnPDE4D3GFP were acquired and cells assigned to the different stages of the cell cycle as defined in A. At least 120 mitotic cells were analyzed for each experiment. Data are expressed as percentage of mitotic cells that appears to be in prophase.

Figure 1

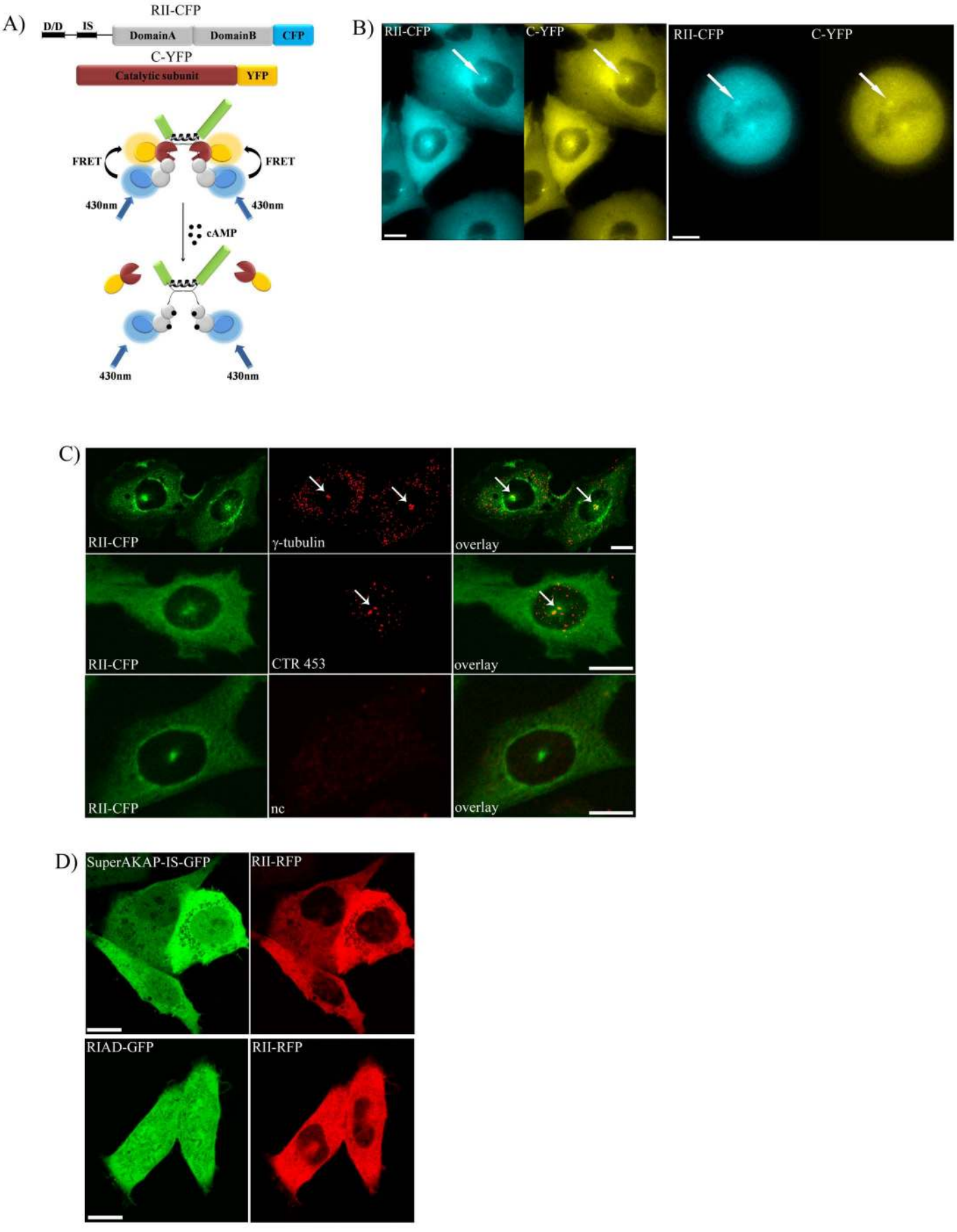
A)
RII-CFP
D/D
IS
DomainA
DomainB
CFP
C-YFP
Catalytic subunit
YFP
FRET
FRET
430nm
430nm
cAMP
430nm
430nm
B)
RII-CFP
C-YFP
RII-CFP
C-YFP
C)
RII-CFP
γ-tubulin
overlay
RII-CFP
CTR 453
overlay
RII-CFP
nc
overlay
D)
SuperAKAP-IS-GFP
RII-RFP
RIAD-GFP
RII-RFP

Figure 2

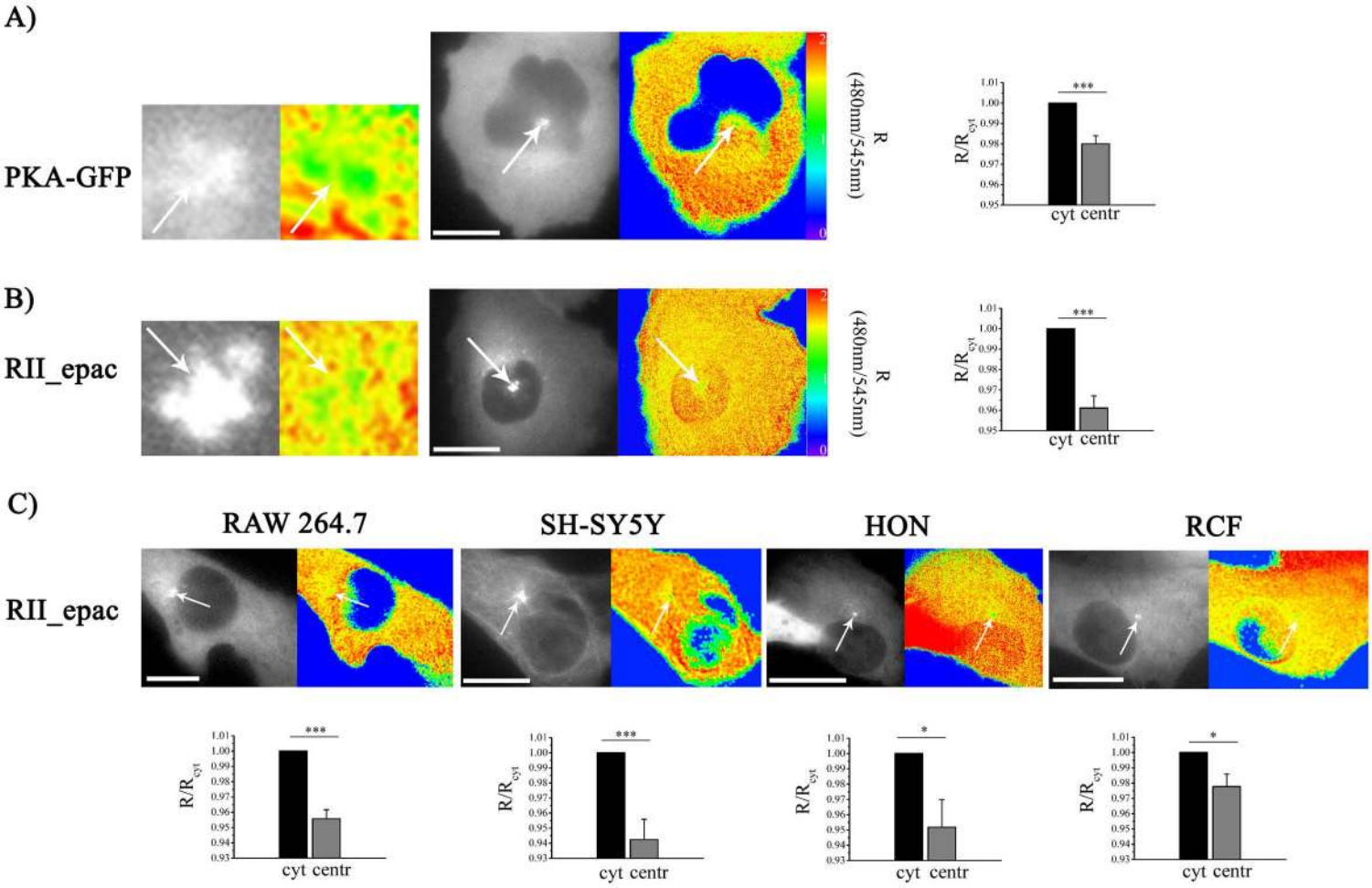
A)
PKA-GFP
R
(480nm/545nm)
R/R$_{cyt}$
***
cyt centr
B)
RII_epac
R
(480nm/545nm)
R/R$_{cyt}$
***
cyt centr
C)
RII_epac
RAW 264.7
SH-SY5Y
HON
RCF
R/R$_{cyt}$
***
cyt centr
R/R$_{cyt}$
***
cyt centr
R/R$_{cyt}$
*
cyt centr
R/R$_{cyt}$
*
cyt centr

Figure 3

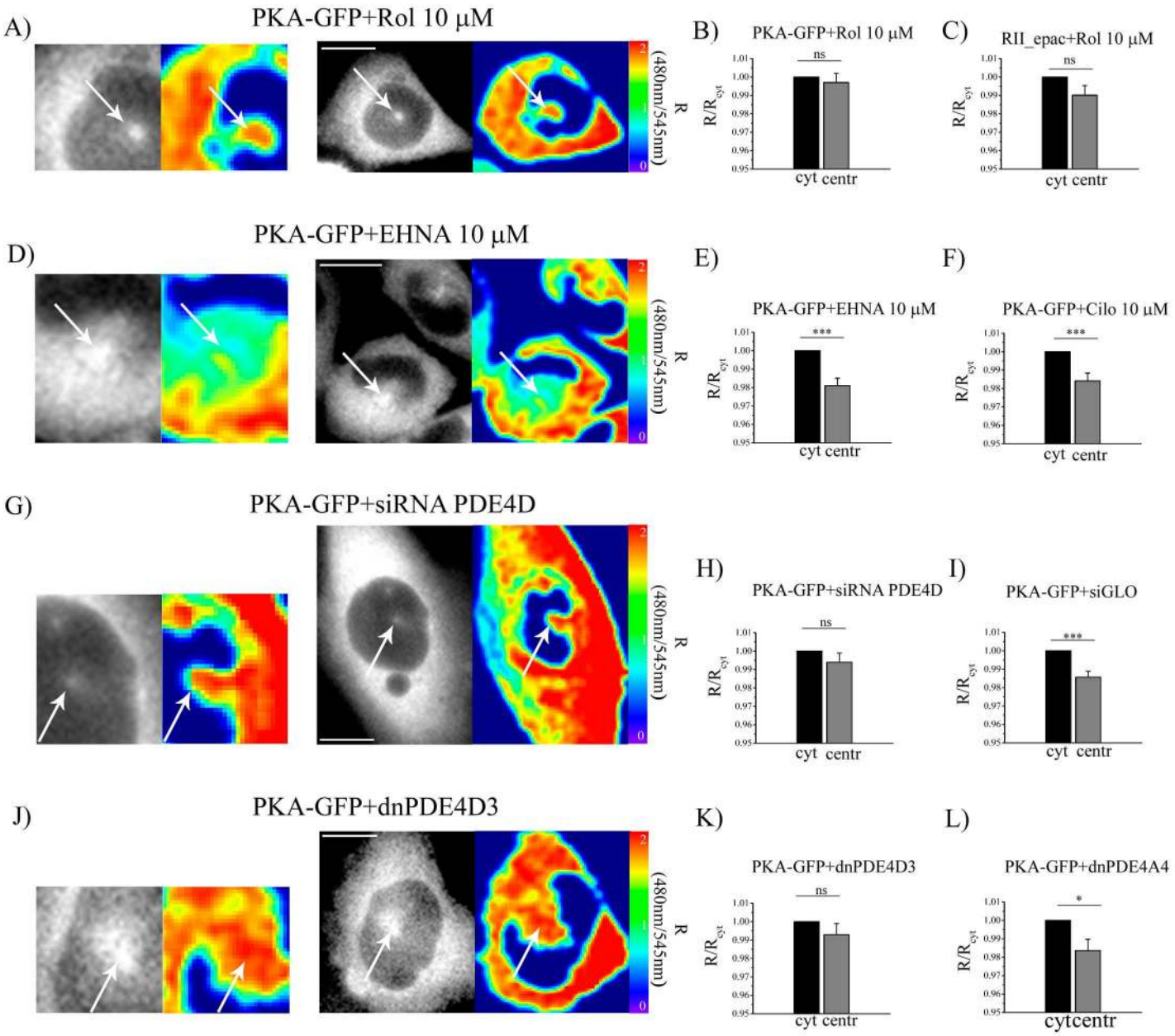
A)
PKA-GFP+Rol 10 µM
R (480nm/545nm)
B)
PKA-GFP+Rol 10 µM
ns
R/R_cyt
cyt centr
C)
RII_epac+Rol 10 µM
ns
cyt centr
D)
PKA-GFP+EHNA 10 µM
E)
PKA-GFP+EHNA 10 µM
***
cyt centr
F)
PKA-GFP+Cilo 10 µM
***
cyt centr
G)
PKA-GFP+siRNA PDE4D
H)
PKA-GFP+siRNA PDE4D
ns
cyt centr
I)
PKA-GFP+siGLO
***
cyt centr
J)
PKA-GFP+dnPDE4D3
K)
PKA-GFP+dnPDE4D3
ns
cyt centr
L)
PKA-GFP+dnPDE4A4
*
cytcentr

Figure 4

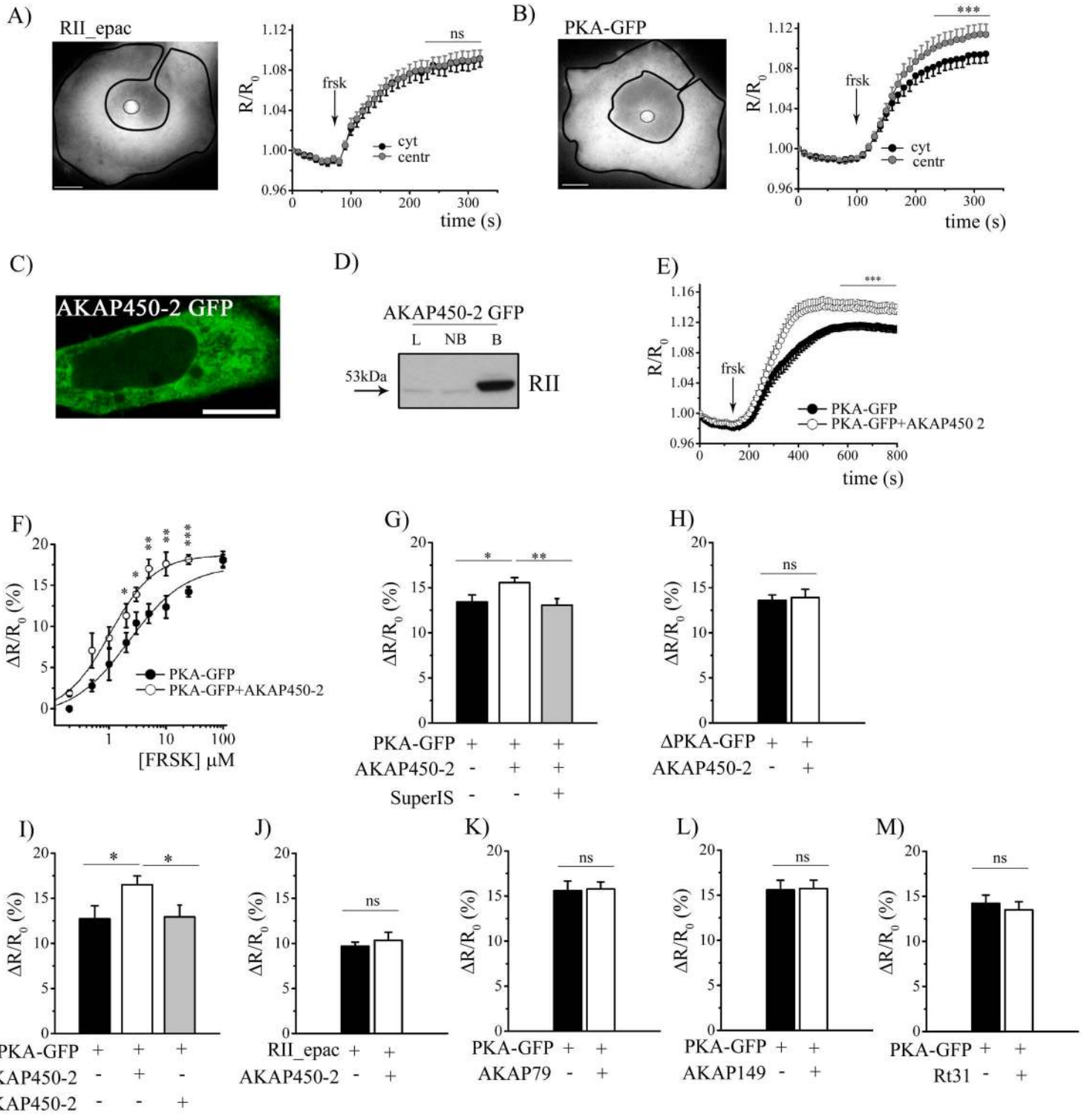
A)
RII_epac
ns
frsk
cyt
centr
time (s)
B)
PKA-GFP
***
C)
AKAP450-2 GFP
D)
AKAP450-2 GFP
L NB B
53kDa
RII
E)
PKA-GFP
PKA-GFP+AKAP450 2
F)
PKA-GFP
PKA-GFP+AKAP450-2
[FRSK] µM
G)
PKA-GFP + + +
AKAP450-2 - + +
SuperIS - - +
H)
ΔPKA-GFP + +
AKAP450-2 - +
I)
PKA-GFP + + +
AKAP450-2 - + -
mutAKAP450-2 - - +
J)
RII_epac + +
AKAP450-2 - +
K)
PKA-GFP + +
AKAP79 - +
L)
PKA-GFP + +
AKAP149 - +
M)
PKA-GFP + +
Rt31 - +

Figure 5

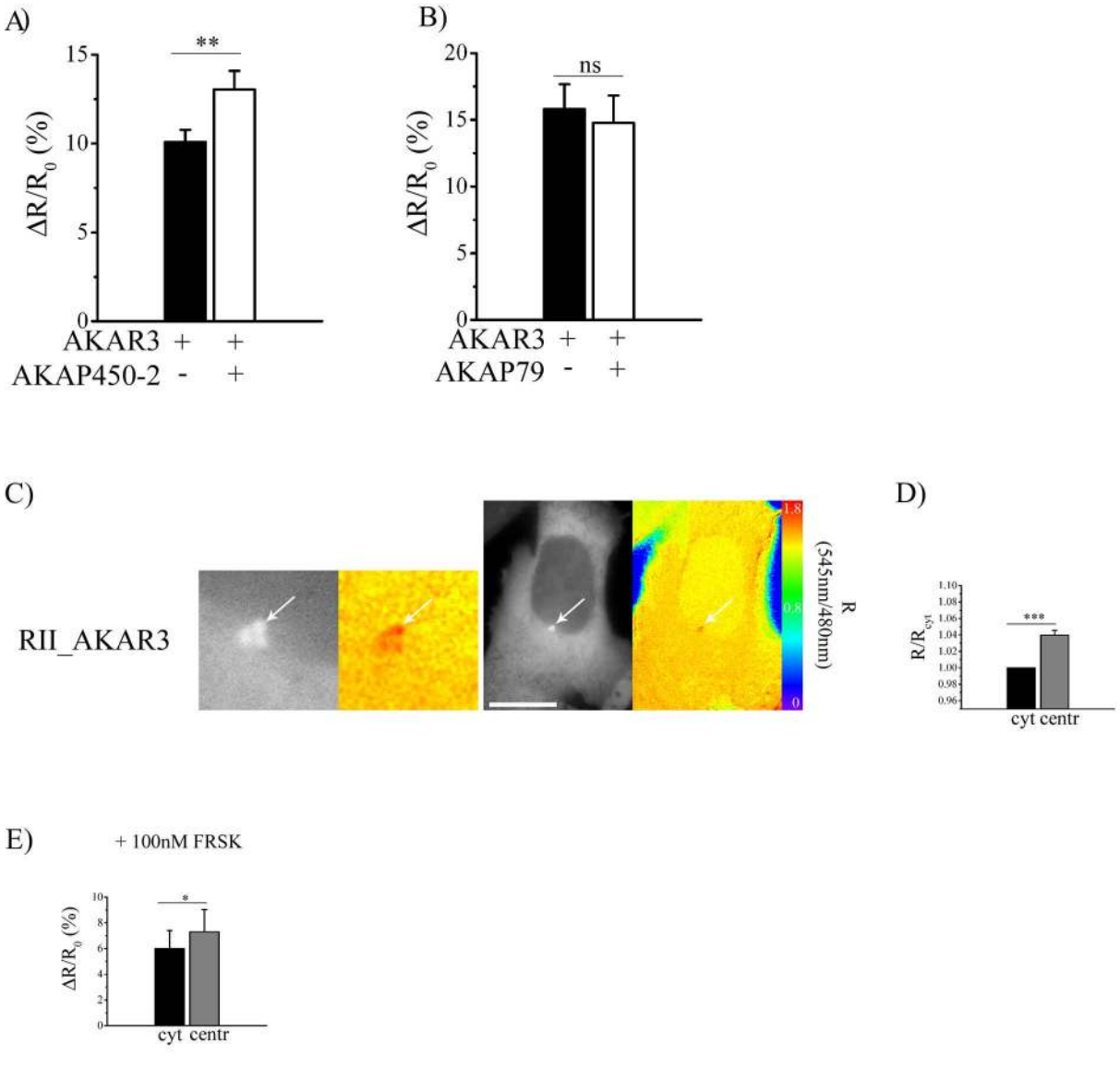
A)
**
ΔR/R0 (%)
15
10
5
0
AKAR3 + +
AKAP450-2 - +
B)
ns
ΔR/R0 (%)
20
15
10
5
0
AKAR3 + +
AKAP79 - +
C)
RII_AKAR3
1.8
0.8
0
R
(545nm/480nm)
D)
***
R/Rcyt
1.10
1.08
1.06
1.04
1.02
1.00
0.98
0.96
cyt centr
E)
+ 100nM FRSK
*
ΔR/R0 (%)
10
8
6
4
2
0
cyt centr

Figure 6

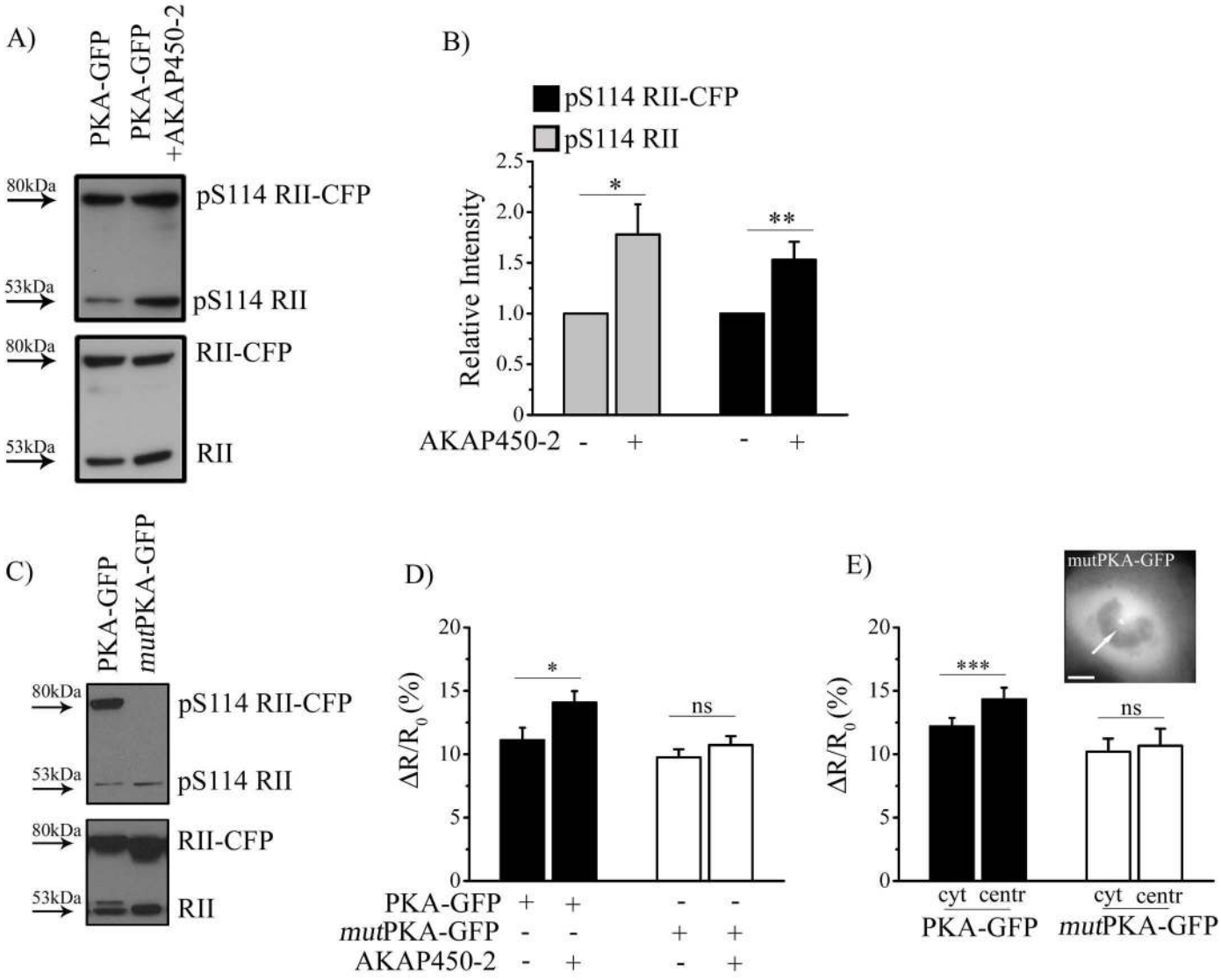
A)
PKA-GFP
PKA-GFP +AKAP450-2
80kDa
53kDa
pS114 RII-CFP
pS114 RII
RII-CFP
RII
B)
pS114 RII-CFP
pS114 RII
Relative Intensity
AKAP450-2
C)
PKA-GFP
mutPKA-GFP
D)
ΔR/R0 (%)
PKA-GFP
mutPKA-GFP
AKAP450-2
ns
E)
mutPKA-GFP
cyt centr
PKA-GFP
mutPKA-GFP

Figure 7

A)

RII_epac
mitosis

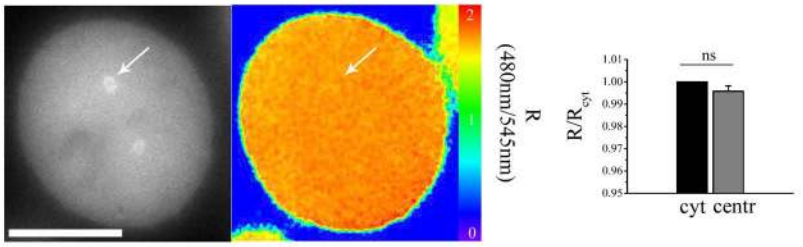

B)

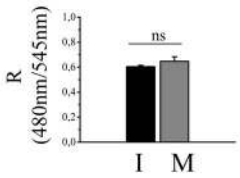

C)

RII_AKAR3
mitosis

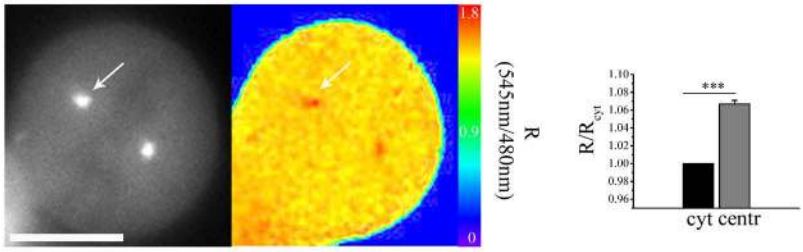

D)

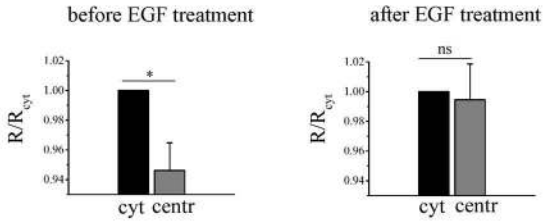

Figure 8

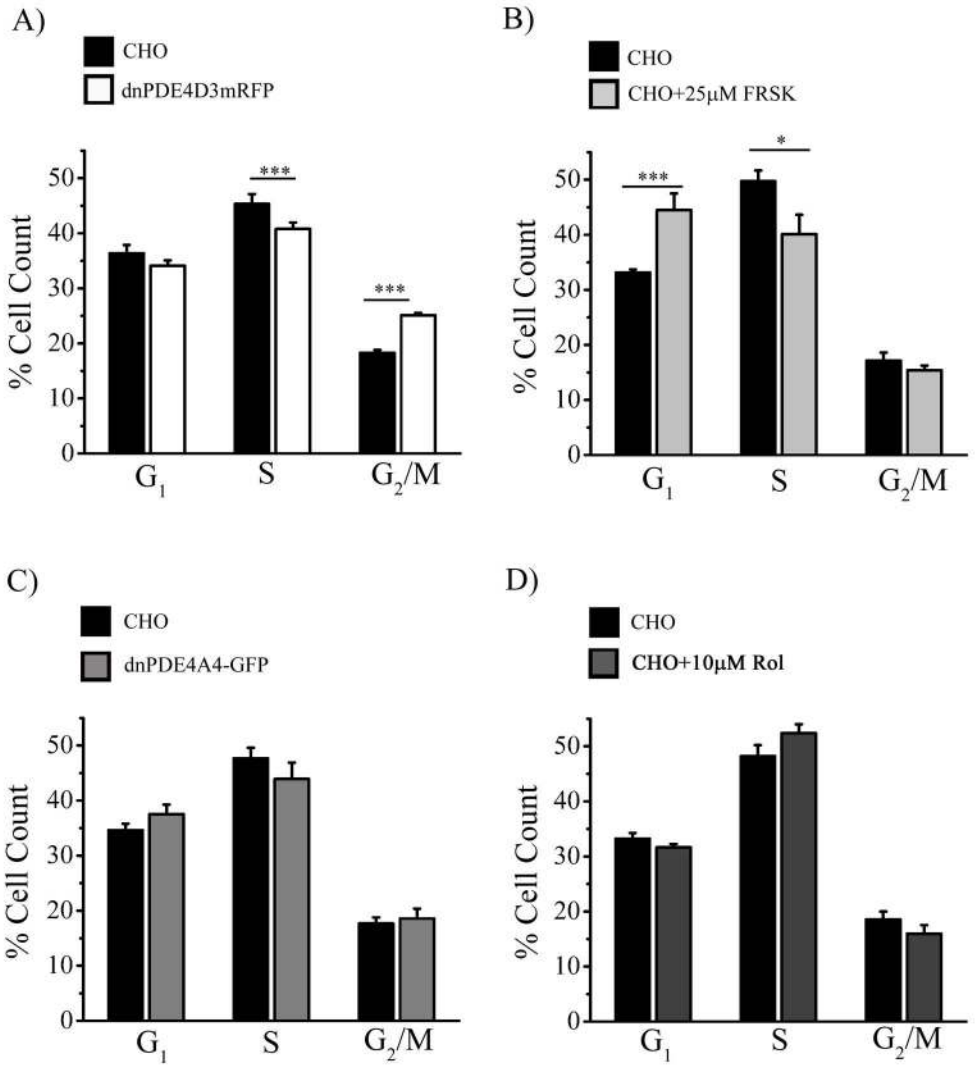
A)
CHO
dnPDE4D3mRFP
% Cell Count
***
***
G1
S
G2/M
B)
CHO
CHO+25µM FRSK
% Cell Count
***
*
G1
S
G2/M
C)
CHO
dnPDE4A4-GFP
% Cell Count
G1
S
G2/M
D)
CHO
CHO+10µM Rol
% Cell Count
G1
S
G2/M

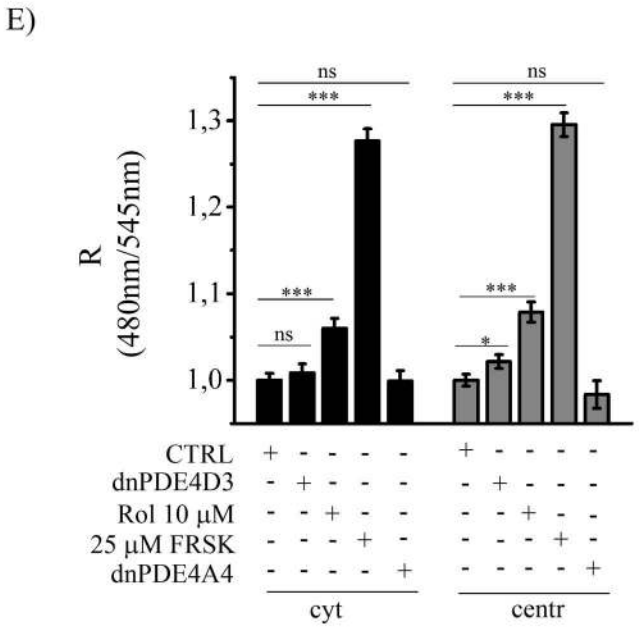
E)
R
(480nm/545nm)
ns
***
***
ns
ns
***
***
*
CTRL
dnPDE4D3
Rol 10 µM
25 µM FRSK
dnPDE4A4
cyt
centr

Figure9

A)

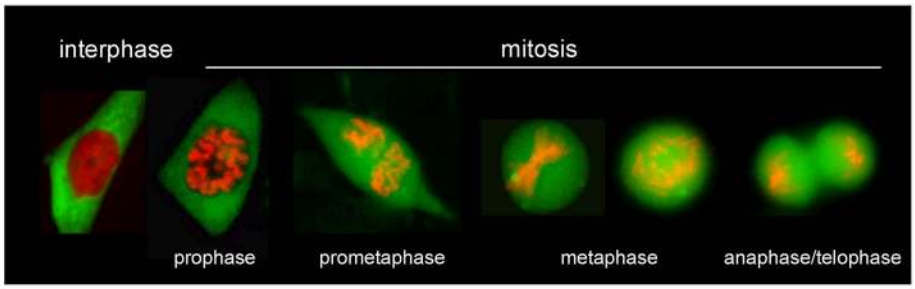
interphase
mitosis
prophase
prometaphase
metaphase
anaphase/telophase

B)

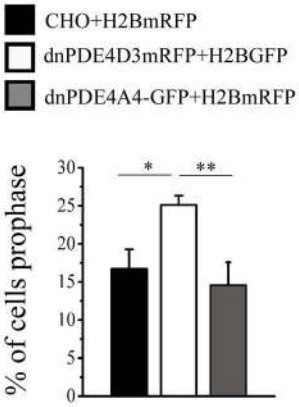
CHO+H2BmRFP
dnPDE4D3mRFP+H2BGFP
dnPDE4A4-GFP+H2BmRFP
% of cells prophase
30
25
20
15
10
5
0
*
**

Supplemental material

Supplementary figure1: **A)** CHO cells transiently expressing the PKA-GFP sensor (right, upper panel) immunostained with the centrosomal marker γ-tubulin (left, bottom panel). The bright field image (BF) is also shown. The right, bottom panel shows the overlay between the PKA-GFP signal, γ-tubulin and DAPI. The γ-tubulin staining clearly show that over-expression of PKA-GFP does not affect centrosome morphology. Size bars = 10µm.

Supplementary figure2: A) Schematic representation of cAMP sensor RII_epac. D/D indicates the dimerization/docking domain; CBD indicates the cAMP binding domain; CFP and YFP are respectively the cyan and yellow fluorescent protein. Similarly to PKA-GFP this sensor shows high FRET in the presence of low cAMP and vice versa. **B)** Schematic representation of AKAP450 (aa 1-3908) and AKAP450-2 fragment (aa 933-1834; highlighted in green) encompassing the amphipatic helix (shown in black). The PACT-domain is also indicated. **C)** Schematic representation of the interaction between the FRET-based sensors and the AKAP constructs used in this study.

Supplementary figure3: A) Image in grey scale shows the subcellular localization of PKA-GFP in RPE1 cells. The FRET signal from the same cell is shown in pseudo-color. Panels on the left show a higher magnification of the centrosomal region. Arrows point to the centrosome. The panel on the right shows the average basal

FRET signal measured in the bulk cytosol (cyt) and at the centrosome (centr) of RPE1 cells expressing the PKA-GFP sensor. FRET values are expressed relative to the FRET value measured in the cytosol. n= 20. Error bars represent SEM. Two tailed; paired t-test, * $p<0.05$; ** $0.001<p<0.01$; *** $p<0.001$. Size bars = 10µm.**B)** Representative RPE1 cell expressing PKA-GFP (middle panel) and immunostained for PDE4D3 (left panel). The overlay between the PKA-GFP and the PDE4D3 signals is shown on the right. Arrows point to the centrosome. Bars size = 10µm. **C)** RT-PCR analysis of PDE4D3 wild type and dominant negative variants in RPE1 cells, RPE1 cells selected for stable expression of dnPDE4D3mRFP, RPE1 cells transiently transfected with dnPDE4D3mRFP and CHO line stably expressing the dnPDE4D3mRFP. The 650 bp band expected from the wild type isoform of the PDE4D3 is detectable in the entire set of samples analysed (left panel), whereas only the RPE1 cells transiently expressing the dnPDE4D3mRFP and the CHO stably expressing the dnPDE4D3mRFP show amplification of the dominant negative variant of PDE4D3. The above data indicate that while in cells transiently transfected with dnPDE4D3mRFP the transgene can be detected, RPE1 cells that have been selected for stable expression of dnPDE4D3mRFP have lost the transgene.

Supplementary figure4: **A)** Representative CHO cell co-immunostained with a PDE4D3 specific antibody (left upper panel) and with the centrosome-specific antibody γ-tubulin (middle upper panel). A negative control (nc) in which the primary antibody is omitted is shown in the bottom panels. The overlay between the PDE4D3 (shown on the left) and the γ-tubulin signal is shown on the right panels. Arrows point to the centrosome. Bars size = 10µm **B)** Representative western blot analysis of

PDE4 expression in CHO cells treated as indicated. Lysates from control CHO cells (CTRL) and CHO cells over-expressing either the small RNA interference of PDE4D (siRNAPDE4D) or the control sequence siGLO (SIGLO) were blotted and probed with specific antibody for PDE4D (top panel) and γ-tubulin (bottom panel). Bands above and below 100kDa correspond respectively to PDE4D5/7 and PDE4D3/8/9 isoforms. γ-tubulin detection (lower panel), indicated by the 50KDa band, was used as a control for the amount of protein loaded. **C)** Upper panels: Representative CHO cell stably expressing the RFP-tagged and catalytically inactive PDE4D3 (dnPDE4D3mRFP, left panel) and transiently transfected with CFP tagged PKA type II regulatory subunit (RII-CFP, middle panel). Lower panel: Representative CHO cell stably expressing the GFP-tagged and catalytically inactive PDE4A4 (dnPDE4A4-GFP, left) and transiently transfected with RFP tagged PKA type II regulatory subunit (RII-RFP, middle). Pictures on the right show the overlay between the two signals. Arrow points to the centrosome. Size bars = 10µm.

Supplementary figure 5: Cell synchronization confirms an arrest of the cell cycle progression in G_2/M of cells expressing the dnPDE4D3. A) Quantification of flow cytometry scan analysis of control CHO cells and CHO cells treated with 10 µM rolipram. **B)** Quantification of flow cytometry scan analysis for CHO and CHO stably expressing the catalytic inactive mutant of PDE4D3 (dnPDE4D3mRFP). Histograms indicate the mean percentages of cells in various phases of the cell cycle. Data are the mean of at least 3 independent experiments. Error bar represents SEM. Two tailed; un-paired t-test, ∗ $p<0.05$; ∗∗ $0.001<p<0.01$; ∗∗∗ $p<0.001$.

Supplementary figure1

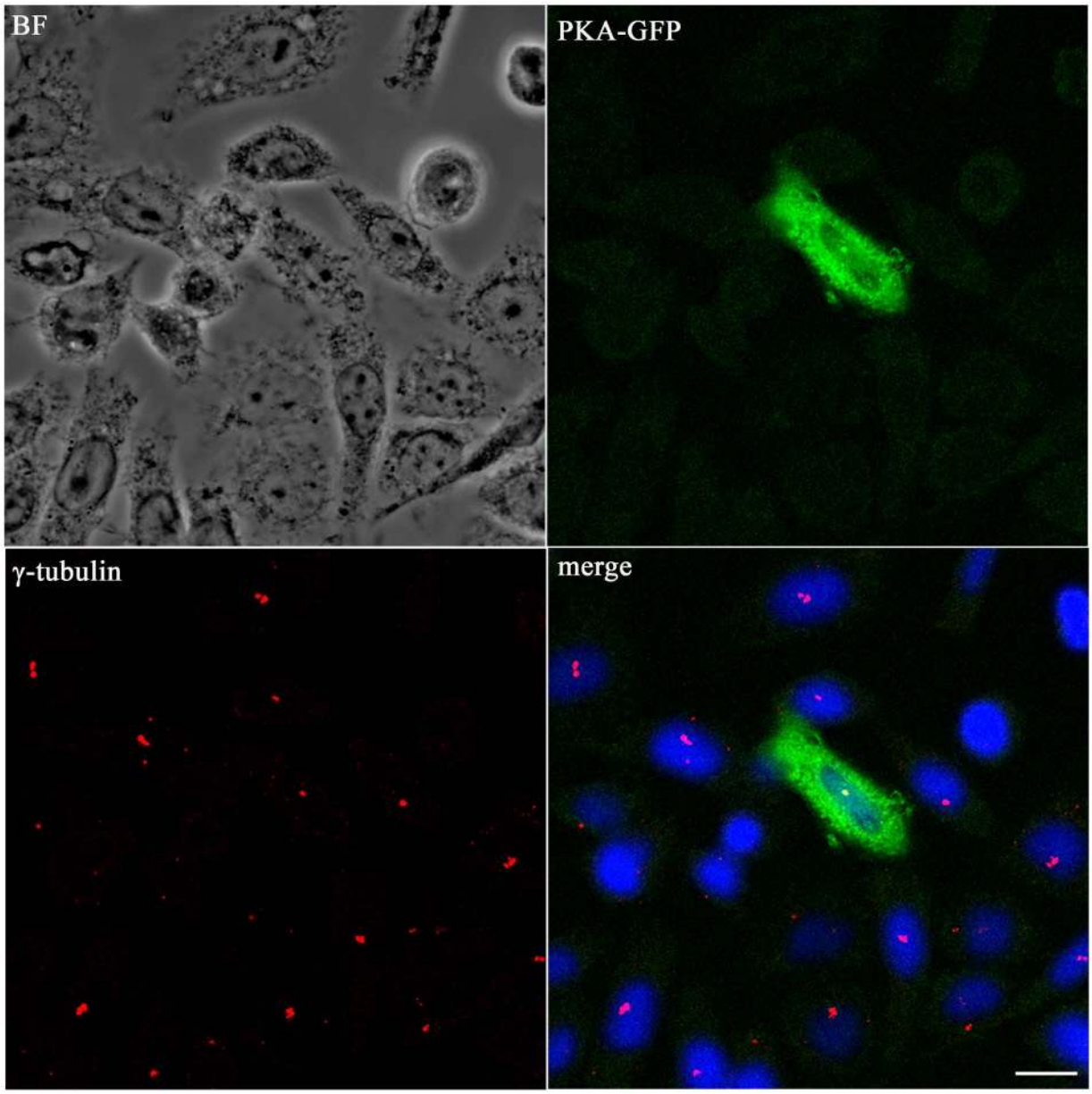

Supplementary figure2

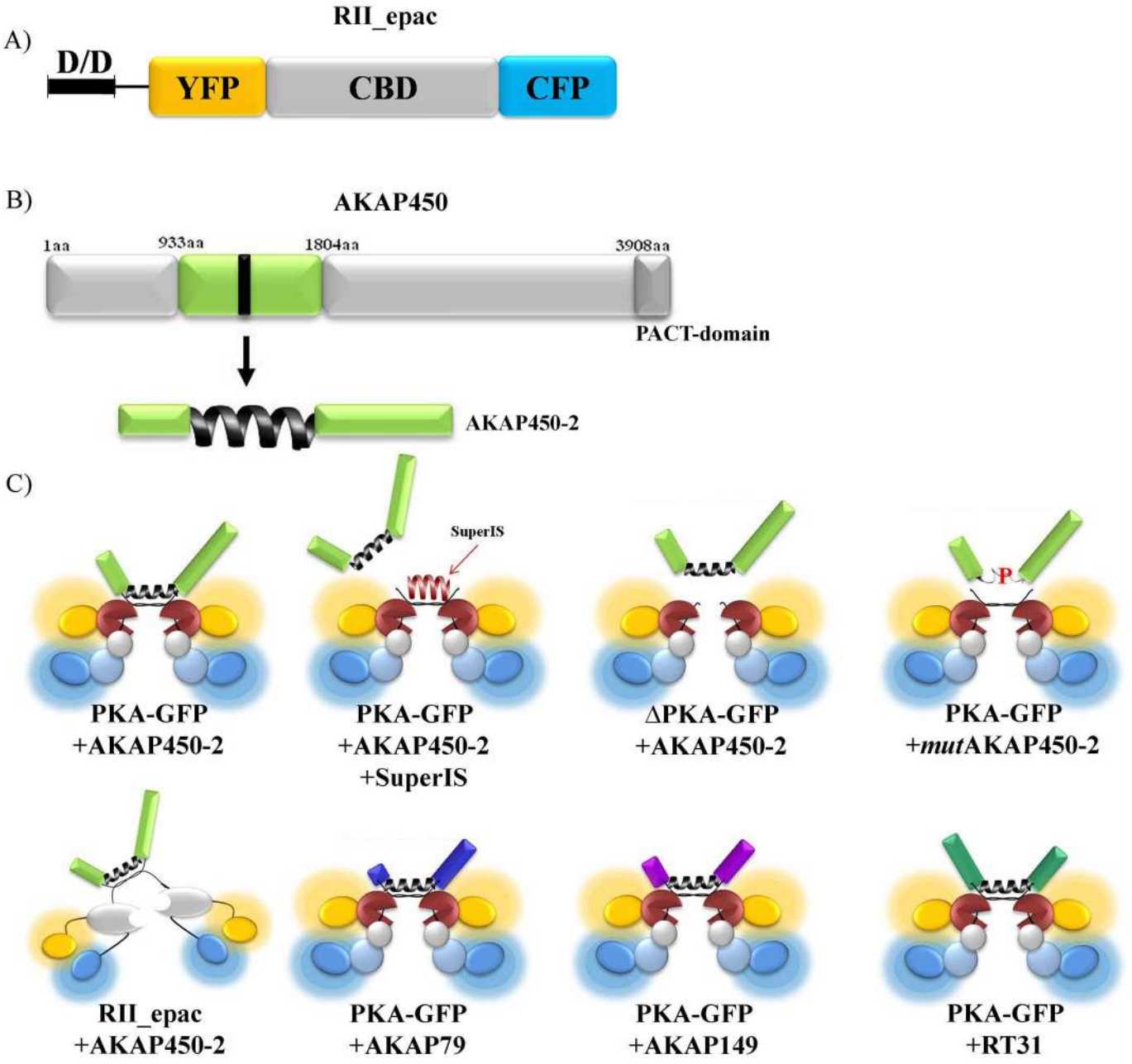

Supplementary figure3

A)

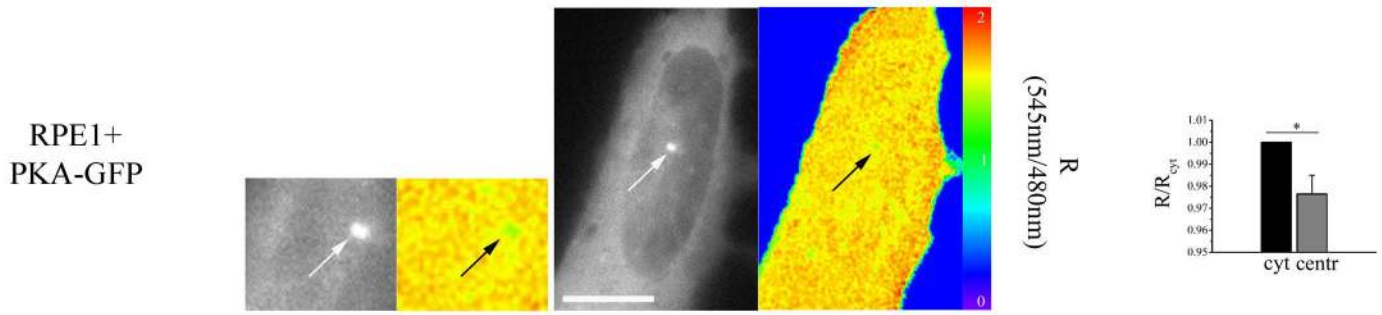

B)

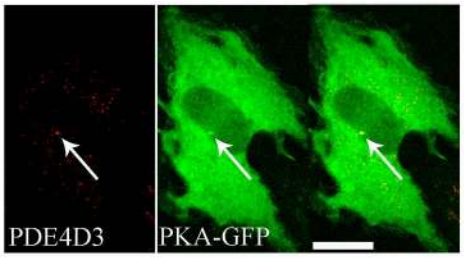

C)

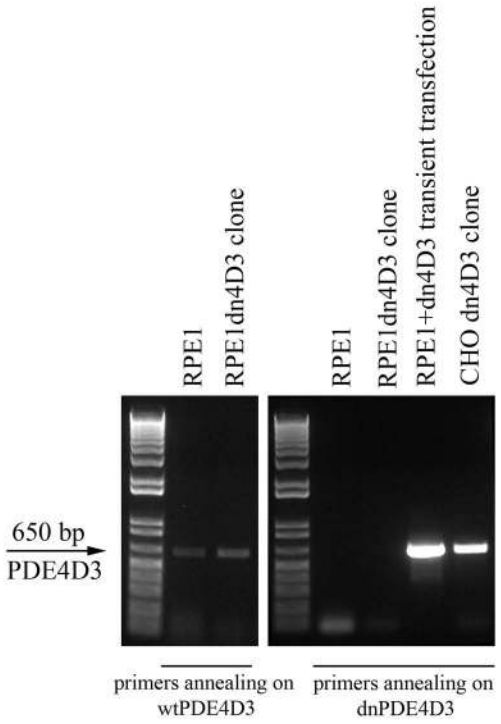

Supplementary figure4

A)

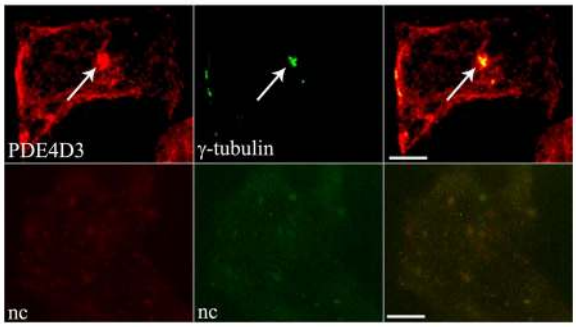

B)

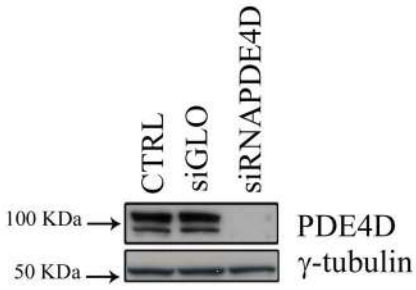

C)

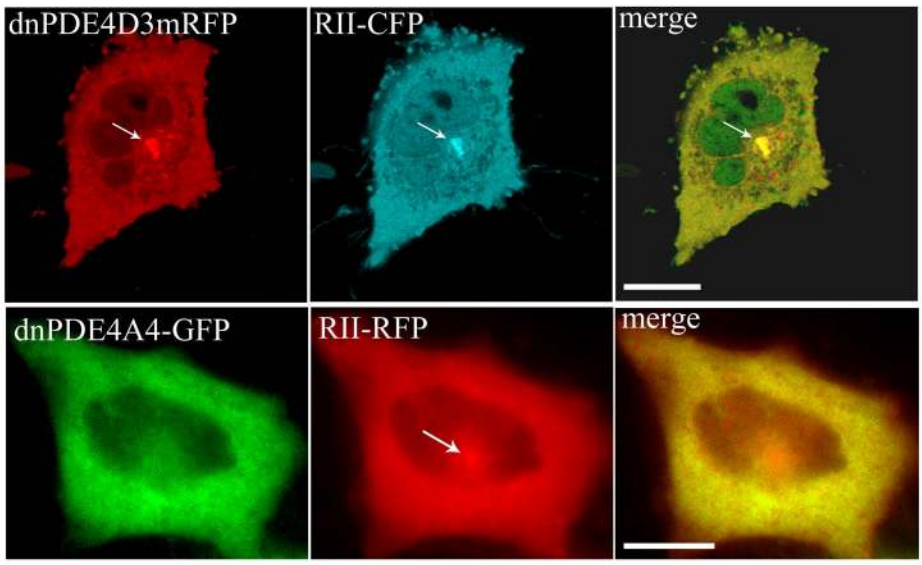

Supplementary figure5

after double block with thymidine